A Theoretical Goaf Resistance Model Based on Gas Production Analysis in Goaf Gas Drainage

Yuehan Wang[1], Guangyao Si[1*], Zizhuo Xiang[1], Joung Oh[1], Bharath Belle[1,2,3,4], David Webb[5]
1. School of Minerals and Energy Resources Engineering, University of New South Wales, Sydney, NSW 2052, Australia;
2. School of Mechanical & Mining Engineering, University of Queensland, Brisbane, QLD4072, Australia
3. University of Pretoria, South Africa
4. Anglo American Metallurgical Coal, Brisbane, QLD 4001, Australia
5. Glencore, Hunter Valley, NSW 2330, Australia

Corresponding author:

*Dr Guangyao Si, g.si@unsw.edu.au

ABSTRACT

Over the past few years, the Australian coal mines heavily relied on drilling vertical goafholes to capture coal mine methane and monitor methane levels, which is named goaf gas drainage. The suction pressure applied on the surface goafholes may change goaf pressure distribution and goaf gas flow pathways. Besides, high suction pressure may cause more air leakage in the goaf and increase the risk of gas explosion and spontaneous combustion, posing a significant threat to mine safety. This paper focuses on analysing goaf gas production data from different goafholes in two active Australian longwall panels. The correlation between suction pressure, total flow rate, gas flow rate and air leakage rate were analysed in detail as the face-to-hole distance changed. Suction pressure is found to be positively correlated with total flow rate, and their correlation also varies at different goaf locations due to various goaf compaction and flow resistance. As a result, instant control strategies are suggested for different scenarios based on adjusting goafhole suction pressure. This paper also proposed a theoretical method to calculate the goaf resistance of ventilation air leakage pathways. The model results suggested that the resistance of air leakage pathways from the working face to individual goafholes increased with the face-to-hole distance, and the resistance results can be used to calculate the corresponding permeability at the same goaf position. These results may be applied to calibrate other geomechanical models and as input data for CFD or Ventsim models with a clear understanding of simulation tool limitations.

Keywords: Goaf Gas Drainage; Suction Pressure; Goaf Resistance; Goaf Permeability

Highlights:

- Goaf gas production data from two case study longwalls were analysed.
- A theoretical goaf resistance model based on gas production analysis was proposed.
- The dynamic control of suction pressure under different scenarios was suggested.
- The application and limitation of the theoretical goaf resistance model were discussed.

1. INTRODUCTION

Coal is a solid combustible energy resource that plays an essential role in developing the global economy. Longwall mining as a continuous and high-productive technique is widely used in many countries to improve underground coal mine productivity, which also accounts for 90% of Australia's total underground coal production. In the mining process, mechanical shears are first operated to cut the coal seam across the longwall working face, and then conveyors are used to transporting the cut and broken coal. In the meantime, hydraulic supports are usually employed to support the roof to protect equipment and workers temporarily. These hydraulic supports move along with the longwall face, resulting in the collapse of overburdens behind the supports (Karacan et al., 2007). The mined area behind the working face is called the 'goaf', filled with broken rocks of various sizes and irregular shapes.

A large amount of coal mine methane released from the undermining coal seam and overlying/underlying layers would enter into the goaf (Karacan et al., 2011). Due to the gradual self-inertisation of the goaf, the methane concentration in the goaf will pass through the explosive range of 5% to 15% (Coward and Jones, 1952). In order to effectively control methane and other harmful gas levels in the goaf, longwall panels normally apply a powerful ventilation system to supply fresh air continuously (Karacan, 2015). Australian underground coal mines usually adopt a typical U-type, bleederless ventilation system, and the working face ventilation intake side is called maingate (MG), and the return airway is called tailgate (TG). Due to the continuous oxygen supply from the working face, residual coal in the goaf can react with the leaked air from the face and accumulate heat, which is one of the main causes of spontaneous combustion in the goaf (Wu and Liu, 2011; Yang et al., 2014). A spontaneous combustion event not only releases a large amount of toxic and harmful gases but may also provide an ignition source for gas explosions in longwall goafs given the ready presence of an explosive gas mixture (Cheng et al., 2017; Xiang et al., 2021).

For gassy mines, ventilation systems may not solve the high gas emission issue alone, and other degasification systems may be required. Goaf gas drainage is a post-drainage method often used to control gas emissions from the goaf during coal extraction. This method involves drilling a series of vertical goafholes from the surface to a certain depth above the under-mining coal seam, usually 10 m to 30 m. A vacuum pump is connected to the goafhole at the surface to drive gas flow from the goaf and overlying fractured strata (Figure 1). Without goaf drainage, coal mine methane will be carried by the ventilation air and released into the atmosphere as greenhouse gases, which is found to be more potent given the warming effect of methane is 28 times that of carbon dioxide (Borunda, 2019). Global

gas emissions from coal mines are estimated to reach 912 $MtCO_2e$ by 2030 (United States Environmental Protection Agency, 2019). Capturing and utilising these fugitive methane emissions can effectively slow down the global warming effect and recover a large amount of energy (Ye et al., 2017).

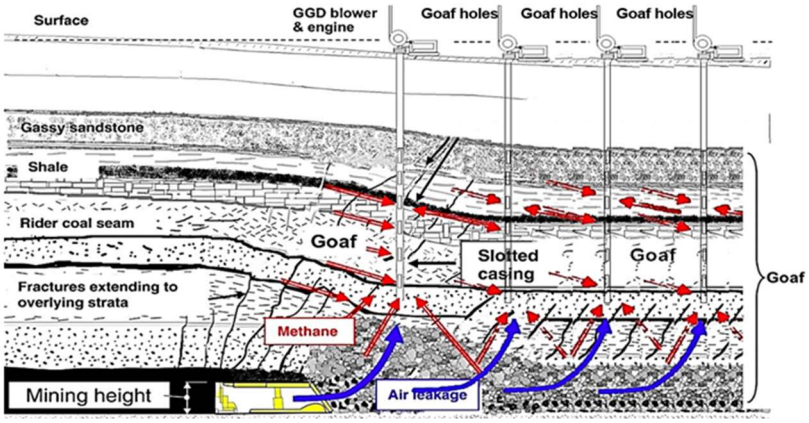

Figure 1. The cross-section of longwall mining with intensive goaf gas drainage (modified from Karacan, 2009b)

However, high suction pressure applied on goafholes may cause goaf air mixtures to enter the explosive range and the expansion of the goaf gas fringe zone. The computational fluid dynamics (CFD) model developed by Ren and Edwards (2002) suggested that increasing suction pressure would aggravate air leakage. Air entering the goaf increases oxidation exotherm and consequently the risk of spontaneous fire. Si and Belle (2019) suggested that suction pressure can be adjusted for different situations based on the results of the field data analysis of gas production data, in favour of maximising gas production rate while maintaining spontaneous combustion risk at a low level. Understanding the impact of suction pressure helps control goaf gas flow and avoid gas explosion and spontaneous combustion incidents.

The distribution of goaf permeability is another important factor that controls gas emissions migration and air leakage pathways into the goaf, and it depends on the goaf compaction degree. Gradually compacted rocks and coal behind the longwall working face facilitate a porous goaf environment, which provides a complex and dynamic migration pathway for the goaf gas (Liu et al., 2020). Karacan (2009b) used the well testing method to analyse the behaviour of six goafholes during and after mining, such as permeability, flow efficiency, and damage ratio, to better understand the operating efficiency of goafholes and the reservoir features of the goaf. On the basis of extensive field tests, a method to determine the permeability of the goaf caved zone formed by different types of roof rock was proposed by (Szlazak, 2001, Szlazak and Szlazak, 2001). This pioneering study shows that the permeability decreases with the increase of the distance to the longwall working face, and there is a linear

relationship between the permeability and goaf distance under the assumption that the airflow in the goaf is laminar. However, because access to unknown goaf environments is commonly challenging, it is difficult to directly measure goaf permeability or the spatial distribution of crushed rocks and coal using conventional methods (Wendt and Balusu, 2002; Esterhuizen and Karacan, 2005, 2007; Whittles et al., 2006; Karacan et al. 2007, 2009a; Chen et al., 2016, Zhang et al., 2019). Many researchers have developed geomechanical models to illustrate the progressive compaction process and then use them to estimate goaf permeability. These results can be used as an input for reservoir models to evaluate goaf gas drainage performance (Esterhuizen and Karacan, 2005, 2007; Esterhuizen et al. 2010; Karacan et al., 2006; Karacan et al., 2007; Karacan, 2009a, 2009b). A similar coupled geomechanics and gas flow modelling approach was also applied in thick seam mines (Si, 2015a; 2015b). Other indirectly methods using microseismic monitoring to infer mining-induced permeability changes were also explored (Zhao et al, 2019, Wang et al, 2021, Duan et al, 2021, Wang et al, 2022). Diamond et al. (1994, 1995) reported high permeability near the edge of the longwall panel as the strata were supported by adjacent pillars, and goafholes near the edge produced 80% more gas than that near the centreline. Based on the numerical modelling results from Guo et al. (2012), permeability was found to increase at the stress-relief zone, and an 'annular' zone with high vertical and horizontal permeability was developed at the goaf area, which is in line with the observation that goafholes near the goaf edge have better gas drainage performance (Zhang et al., 2016; Zhang et al., 2019). As Figure 2 shown, the permeability distribution obtained from geomechanical models conforms to the O-shape distribution in the goaf. Moreover, some Chinese researchers analysed the influences of different permeability distributions on the airflow pathways and gas distributions in the longwall goaf using numerical modelling (Gao and Wang, 2010; Gao et al., 2013). As a result, the permeability distribution may affect the accuracy of other numerical models where it is used as input data.

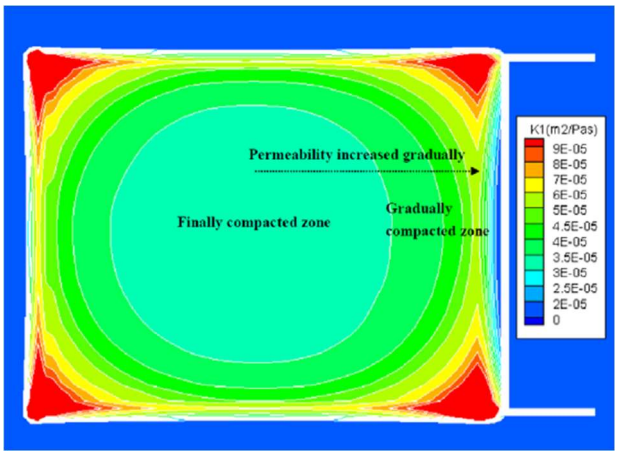

Figure 2. The plan view of a fully caved goaf permeability distribution (Zhang et al., 2016)

The increasing capacity of goaf gas drainage in high gassy mines may cause more air leakage in the goaf, which may lead to increased risks of spontaneous combustion and gas explosion. This has been clearly explored and discussed in our previous publication (Xiang et al., 2021), which focused on the gas composition analysis of goaf gas drainage data and determining goaf atmosphere change during the dynamic longwall mining. Based on extensive goaf gas drainage data analysis from two case study mines in Australia, a conceptual goaf gas atmosphere model with the consideration of goaf drainage impact has been proposed, which can be used to assess the spontaneous combustion and gas explosion risks in the goaf.

As a continuation to our previous paper in 2021, this paper is based on hundreds of goafholes production data from the same field to analyse the correlation between the suction pressure and gas flow rate, as well as the goaf gas emission and air leakage trend along the TG and MG side goaf in two case study longwall panels. Based on these data analysis results, the instant feedback strategies to improve goaf gas capture by controlling suction pressure have been proposed. This study also established a theoretical resistance model to calculate the airflow resistance from the face to the goaf, which can be used to infer goaf permeability and optimise gas drainage performance.

2. MINE SITE CONDITIONS

Goaf drainage data analysed in this study were collected from two adjacent longwall panels (LW A and LW B) in a typical gassy coal mine in Australia. The studied mine used the longwall mining method to extract the target coal seam, which has an average thickness of 2.6 m. Furthermore, the coal seam is overlain by a 20 m thick sandstone with 10-20% porosity, and Figure 3 (a) shows a detailed stratigraphic map reflecting the adjacent strata of the target coal seam (Xiang et al., 2021). Gas emissions from the coal seam at the mine range from 5 to 25 m^3/t, which consist of 10% free gas and 90% adsorbed gas. The main component of coal seam gas is CH_4, which accounts for over 90% of total emissions, and the remaining gas is CO_2. The two adjacent panels (LW A and LW B) analysed in this study have a width of approximately 350 m, with lengths of 4200 m and 3400 m, respectively. Both panels use a conventional 'U' ventilation system with the quantity of air flowing through longwall workings at approximately 40-60 m^3/s.

To ensure a safe working environment for the longwall face, a series of vertical goafholes were drilled from the surface to capture goaf gas emissions. Figure 3 (b) shows the layout of the goafholes in both longwall panels that are analysed in this research. There were 84 vertical goafholes distributed in the

LW A panel. As shown in Figure 3, 73 goafholes evenly distributed along the panel length with 50 m intervals and around 30 m offset from the TG edge, and these goafholes are marked as A-TG01 to A-TG73. Besides, 7 goafholes (A-MG01 to A-MG07) located 30-50 m away from the MG side, and their spacing ranges from 200-700 m. Like the TG goafholes in LW A, 53 goafholes were uniformly distributed at the TG side of LW B, which are denoted as B-TG01 to B-TG53 from the inbye to outbye. There were also 9 goafholes (B-MG01 to B-MG09) on the MG side of LW B with various spacings from 90 m to 1100 m. Goafholes drilled at the installation road (A-01 to A-04; B-01 to B-03) will not be analysed in this study, as their positions are significantly different from other goafholes along with the TG and MG sides and their operation lifetimes are also short. In the early stages of the LW A and LW B retreats, TG goafholes started operation after the longwall working face passing by 15-40 m, and this distance increased to 120-150 m later for outbye goafholes.

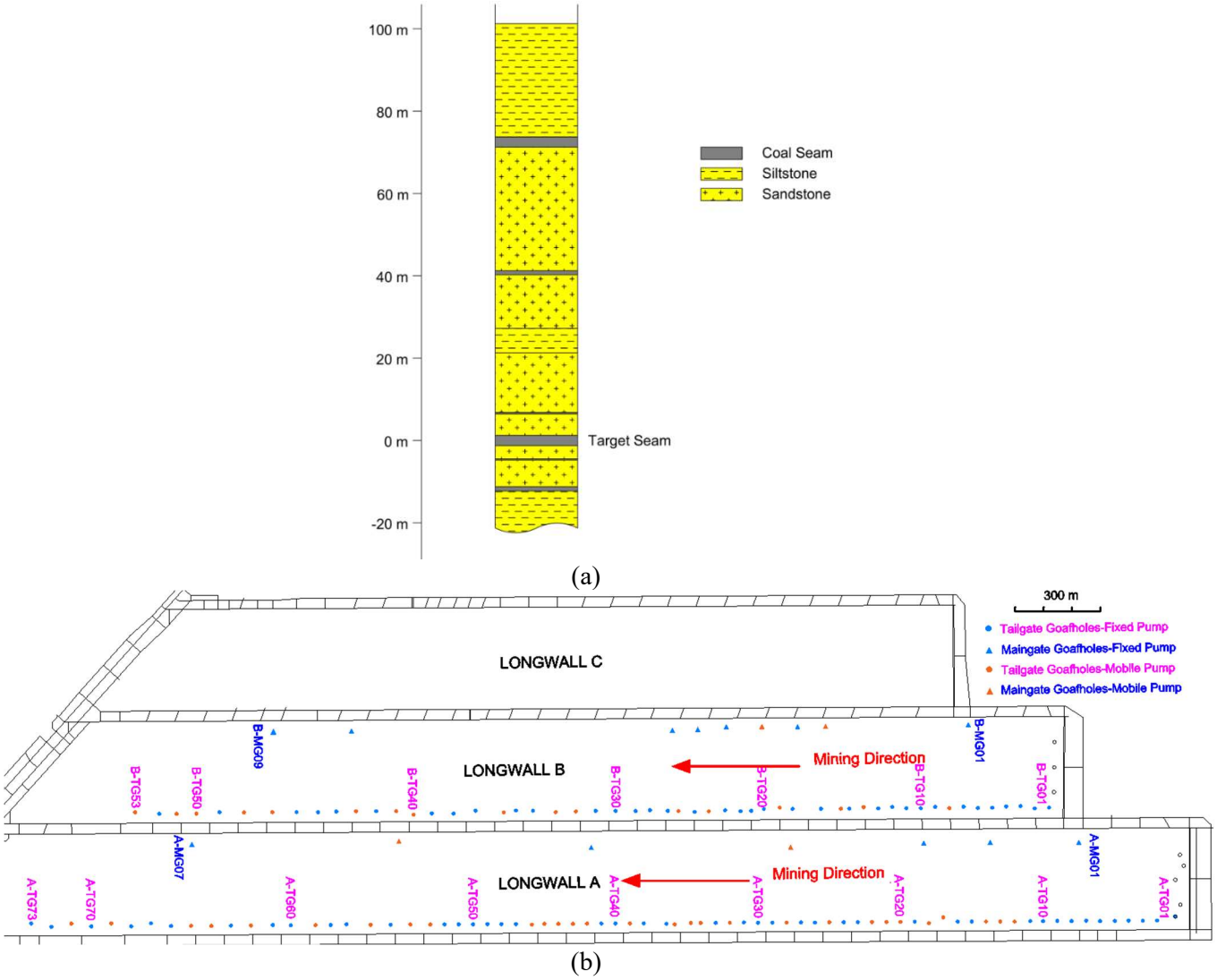

Figure 3. (a) The stratigraphic map of the target coal seam and adjacent strata (b) The plan view of the layout of goafholes in the study mine (Xiang et al. 2021)

The vertical goafholes applied in LW A and LW B are similar to those introduced by Si and Belle (2019). These goafholes were 250 mm in diameter and ~300 m in length, and they were completed approximately 10 m above the top of the target coal seam. The top section of these goafholes is covered by a typical steel surface casing with cement filled between them. The bottom 48 m of the goafholes were cased with slotted steel liner pipes to allow gas inflow. The suction pressure is applied by the gas vacuum pump placed on the surface to extract gas emissions from the goaf and overlying strata. Please refer to Si and Belle (2019) for more detailed goafhole completion information.

Intensive gas monitoring systems were applied in this study mine, including handheld gas monitors, telemetric gas sensors, and sample bag testing. A dedicated seam gas management team used handheld devices to measure CH_4, O_2, CO, and CO_2 concentrations from all operating goafholes in every 4 hours interval. Furthermore, this mine used two different pumping systems, i.e., the fixed pump (central gas drainage plant) and the mobile pump (venturi on a trailer), which were both equipped with pressure transducers to measure static pressure and velocity pressure in each goafhole. The suction pressure for the goafholes controlled by the fixed pump ranged from -2 kPa to -14 kPa, whereas that for mobile pump was lower, between -2 kPa and -8 kPa. The rest of operating parameters for these two pump types are largely similarly. As shown in Figure 3 (b), all the goafholes on the TG and MG sides that were connected with fixed pumps are shown in blue, and the rest of the goafholes controlled by mobile pumps are shown in orange. The gas monitoring systems were flexibly used to monitor continuously changing data from different goafholes in LW A and LW B during the entire production period.

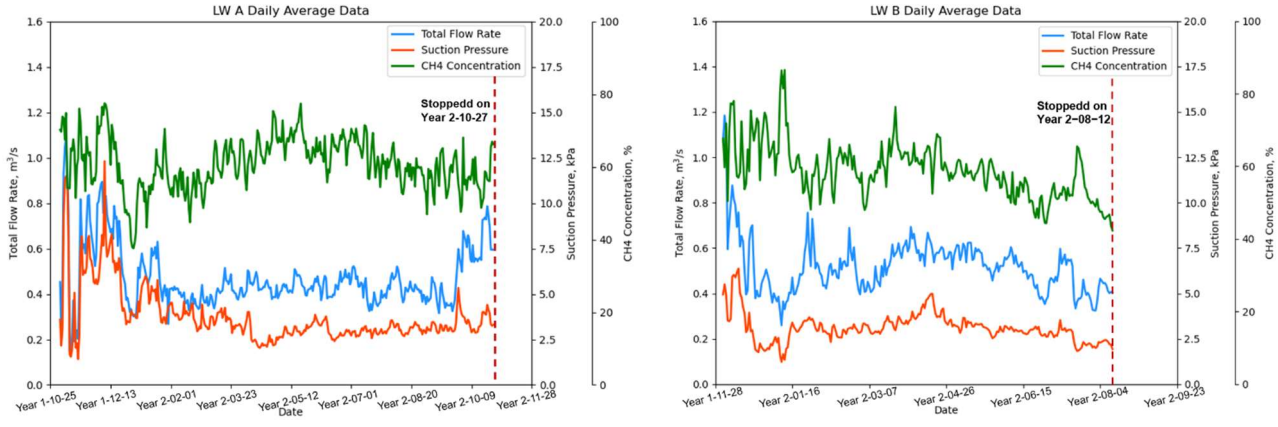

(a) (b)

Figure 4. The daily average data from gas monitoring systems for goafholes in (a) LW A and (b) LW B

The daily average values of total flow rate, suction pressure and CH_4 concentrations of all operating goafholes throughout the LW A and LW B mining periods are shown in Figure 4. A detailed analysis will be performed in the following sections using the mean value of the data collected at different times

during the day, and the different gas contents extracted each day from different goafholes have been presented in detail in Xiang et al. (2021), and thus will not be repeated here.

3. ANALYSIS ON GOAF GAS PRODUCTION DATA

3.1 The Relationship between Suction Pressure and Flow Rate

Suction pressure was measured on each production date as the difference between the barometric pressure and the static pressure head applied on each goafhole. Note that the absolute value of suction pressure is used for plotting purposes in this study, although suction pressure is always in the negative domain. In order to understand the influence of the suction pressure on the goaf drainage flow rate change, the following part will analyse the gas production data collected from both longwall panels. Suction pressure against flow rate from all goafholes in LW A and LW B are scatter-plotted in Figures 5 and 7. In addition, examples of flow rate and suction pressure variation in individual goafholes throughout their whole operation life are shown in Figures 6 and 8.

Figure 5 (a) and (b) show the relationship between suction pressure and flow rate measured from goafholes in the TG and MG sides of LW A, respectively. The blue points in the figure represent the suction pressure applied by the fixed pump, and the orange points represent the pressure driven by the mobile pump. Compared with the fixed pump, the suction pressure applied by the mobile pump would generally result in a lower flow rate (less than 0.5 m^3/s). Most of the data points in the two figures are concentrated near a straight line, showing a positive linear correlation. At the same suction pressure, the flow rate through TG holes is more than that through MG holes, as evidenced by the steeper slope of the MG side linear fitting line in Figure 5 (b). This may indicate better gas drainage performance and higher efficiency in TG holes. The flow rate in goafholes A-TG54 and A-MG06 are plotted against suction pressure over their production period, as shown in Figure 6. The fluctuation of suction pressure is closely related to flow rate change in these two goafholes: higher suction pressure results in higher total flow. Besides, the amount of air ingress also increased along with the total flow rate as expected.

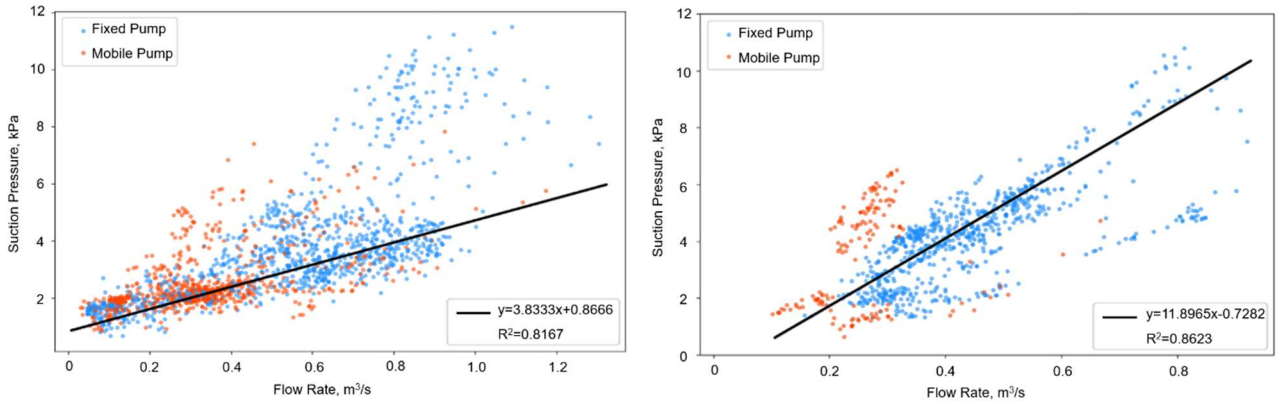

(a) (b)

Figure 5. The relationship between suction pressure and flow rate for goafholes in LWA: (a) TG goafholes and (b) MG goafholes

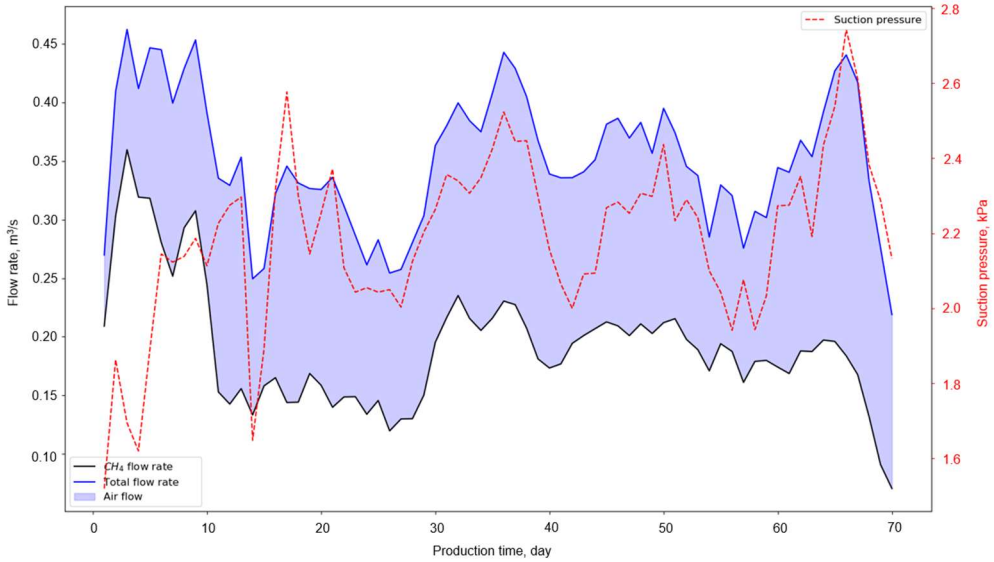

(a)

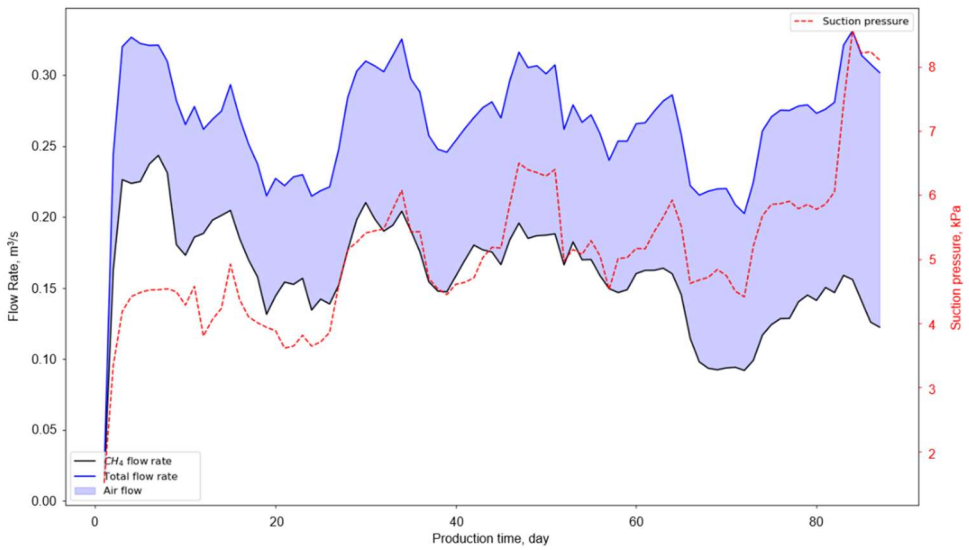

(b)

Figure 6. Variation of flow rate against suction pressure in goafholes (a) A-TG54 and (b) A-MG06 at LWA

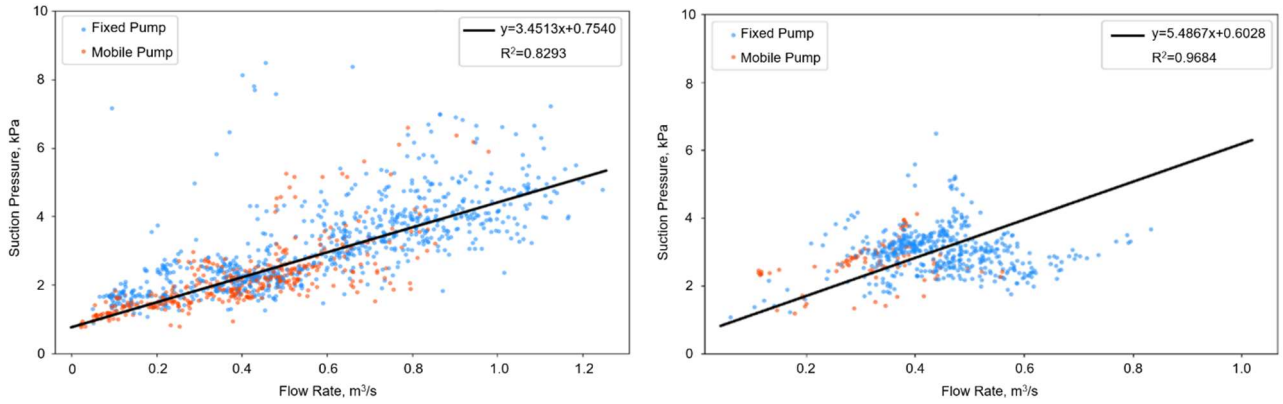

(a) (b)

Figure 7. The relationship between suction pressure and flow rate for goafholes in LWB: (a) TG goafholes and (b) MG goafholes

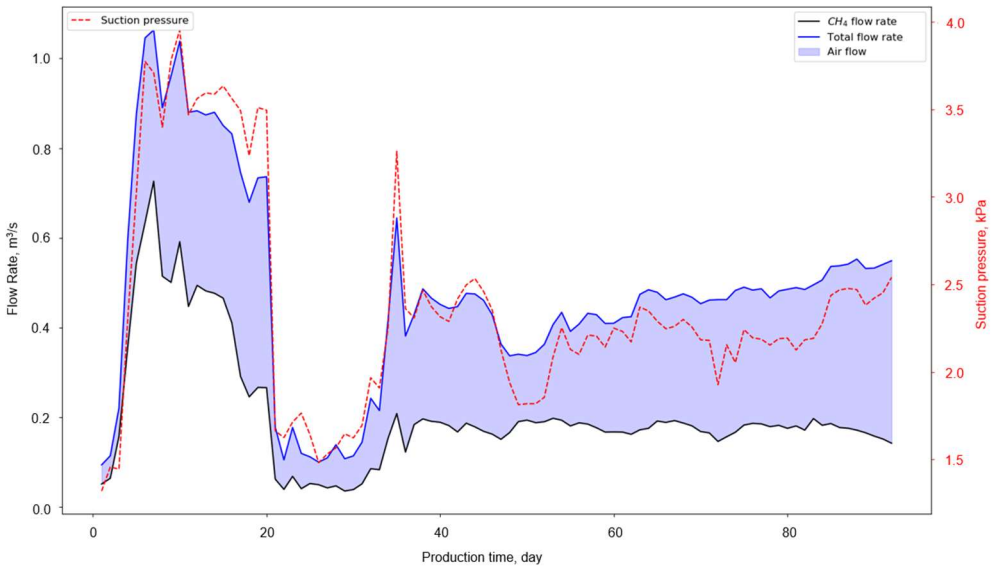

(a)

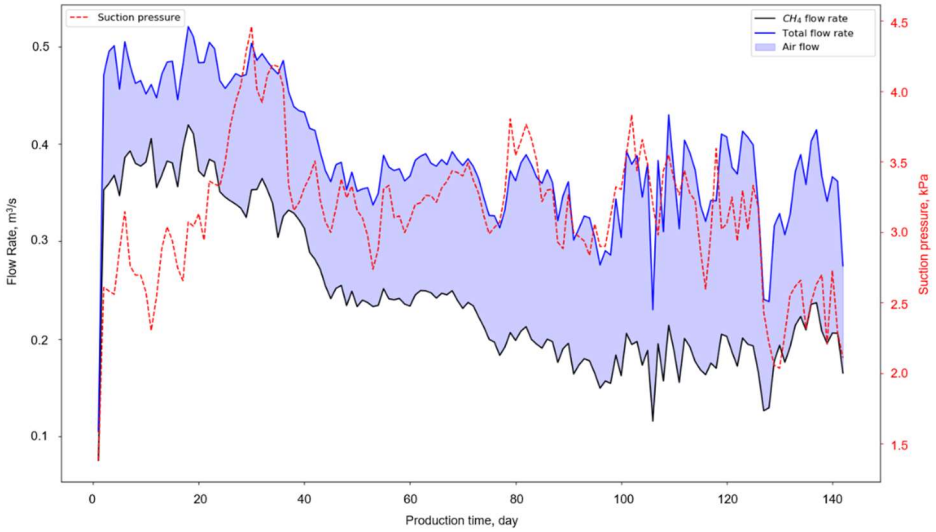

(b)

Figure 8. Variation of flow rate against suction pressure in goafholes (a) B-TG45 and (b) B-MG06 at LWB

The suction pressure changes with the flow rate in the TG and MG goafholes of LW B are shown in Figure 7 (a) and (b), respectively. The positive relationship between the suction pressure and flow rate is similar to that observed in LW A. In LW B, the linear fitting curve obtained from TG goafholes also has a gentler slope than MG goafholes. When the suction pressure changes by 2 kPa, the flow rate change on the TG side is about 0.6 m^3/s. While the flow rate change for the MG goafholes is much smaller, at about 0.3 m^3/s. Based on the gas production curves over the entire period of individual goafholes B-TG45 and B-MG06 in Figure 8, a positive correlation of the suction pressure and total flow rate can be observed. For most of the goafholes, the suction pressure is applied at a relatively low level at the beginning, and then it is increased and adjusted according to the purity of captured gas. As Figure 8 (a) shows, the goafhole B-TG45 had a presence of O_2 above 8% at around 20 days, and the applied suction pressure was then abruptly reduced to control O_2 content in the goaf from exceeding the 10% trigger value.

The goaf filled with collapsed gravel and remaining coal can be viewed as a porous medium for gas and ventilation airflow. The gas flow regime varies significantly in the goaf with the advancing working face and progressive goaf compaction. Many researchers have found that there are turbulent, transitional, and laminar flow zones presenting from the face to the deep goaf (Schmal et al., 1985; Akgun and Essenhigh, 2001; Wu et al., 2007; He et al., 2008). Turbulent and transitional flow is normally observed in the area that is close to the working face, because of the fast ventilation air infiltration into the uncompacted or not fully caved goaf. As moving back into the deep goaf, the air flush effect or momentum gradually diminishes, resulting in the change of flow regime from turbulent to laminar. White (2017) roughly estimated the Reynolds number (Re) is less than 8.4 in the deep goaf based on Eq. 1, which supports the laminar flow assumption in the deep goaf. This conclusion suggests the fluid flow regime in the goaf can be described by Darcy's law (Eq. 2), which is also evidenced by the linear relationship between the suction pressure and flow rate as shown in Figures 5 and 7. Therefore, the laminar flow assumption will be used in the following goaf flow analysis.

$$Re = \frac{\rho u d}{\mu} \quad \text{(Eq. 1)}$$

where, ρ (kg/m^3) is the fluid density; u (m/s) is the fluid mean velocity; d (m) is the mean diameter of an airway; μ ($N{\cdot}s/m^2$) is the fluid viscosity.

$$\Delta P = -\frac{\mu}{k} v \quad \text{(Eq. 2)}$$

where, ΔP (Pa) is the pressure drop; v (m/s) is the fluid velocity through the porous medium; k (m^2)

is the permeability of the porous medium (goaf).

3.2 Gas Emission and Air Leakage Rate in the Active Longwall Goaf

As shown in Figures 9 and 10, the gas emission and air leakage rate in LW A and LW B vary with the distance between goafholes and the working face, which is defined as the face-to-hole distance for future reference. There is a large difference between the production duration of the TG goafholes and MG goafholes. The average active time of TG goafholes is 28 days, and the highest period is about 100 days, while the production period of MG goafholes is much longer, from 10 days up to 250 days. Based on the 14 m/day face advance rate, this research mainly focuses on the face-to-hole distance between 0 to 800 m at the TG side and between 0 to 2000 m at the MG side. The blue triangles in Figures 9 and 10 represent the scatter plot of the total flow rate measured on each date from individual goafholes. The total flow rate here includes both ventilation air leakage and seam gas emission (CH_4 and CO_2). The seam gas flow rate is equal to the total flow rate multiplying the proportion of total CH_4 and CO_2 concentration in captured gas, as indicated by the orange dots in Figures 9 and 10. To smooth the scatter plots, from the face into the goaf, the blue triangles were averaged per 20 m at both the TG and MG sides to obtain the total flow rate trend (as denoted by the solid blue line). Similarly, the trend for seam gas flow rate was obtained and denoted as the solid black line. The area between the solid blue line and the black line is shaded in blue, representing the amount of air leakage (excluding seam gas, thus mainly contains O_2 and N_2) captured by goafholes, which is mostly migrated from the face ventilation. This section will also analyse the suction pressure (dotted red line) impact on the flow rate and the composition change of ventilation air leakage, as indicated by the O_2/N_2 ratio (dotted green line).

Figure 9 (a) shows the flow rate and suction pressure measurement results from TG goafholes in LW A, taking the face-to-hole distance as the abscissa. The total flow rate rises rapidly and reaches a peak of 0.6 m^3/s at approximately 120 m from the working face. Then the total flow rate slowly decreases to around 0.2 m^3/s at 800 m. The seam gas flow rate has the similar trend as the total flow rate. The suction pressure of TG goafholes is positively correlated with the flow rate except for a few high suction pressure points near the working face. Within 120 m from the face, increasing suction pressure will result in more air captured by goafholes. The air leakage amount remained stable between 120 m to 550 m and decreased slightly after 550 m.

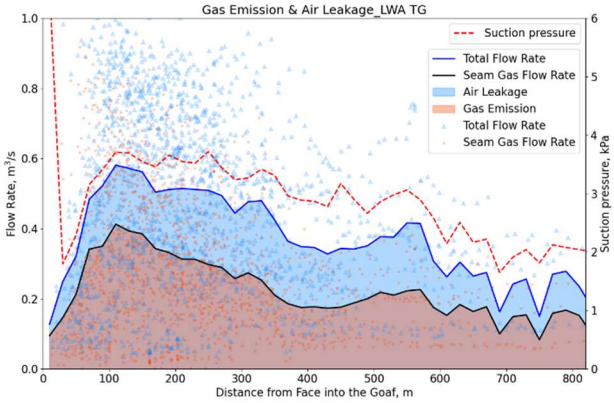

(a)

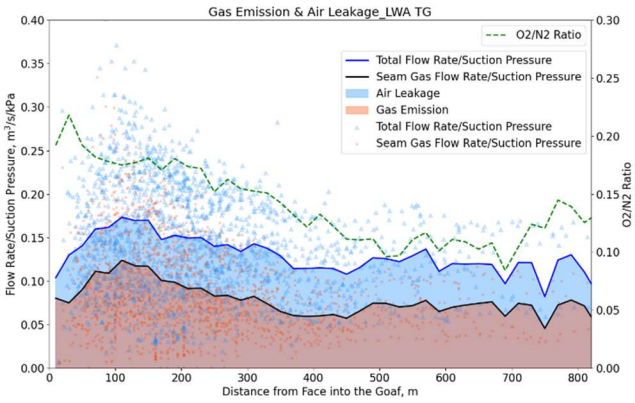

(b)

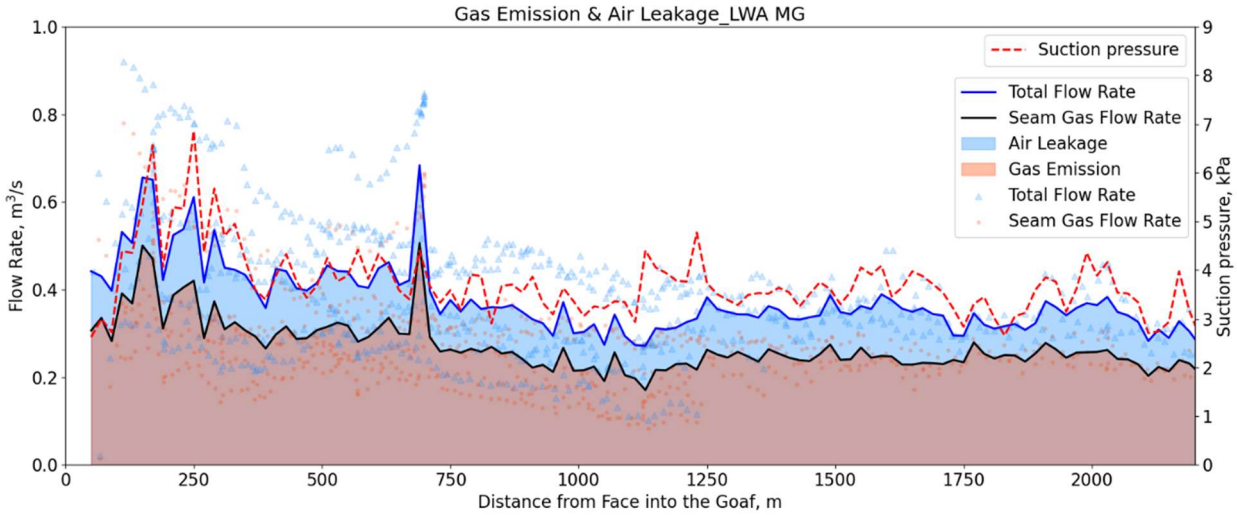

(c)

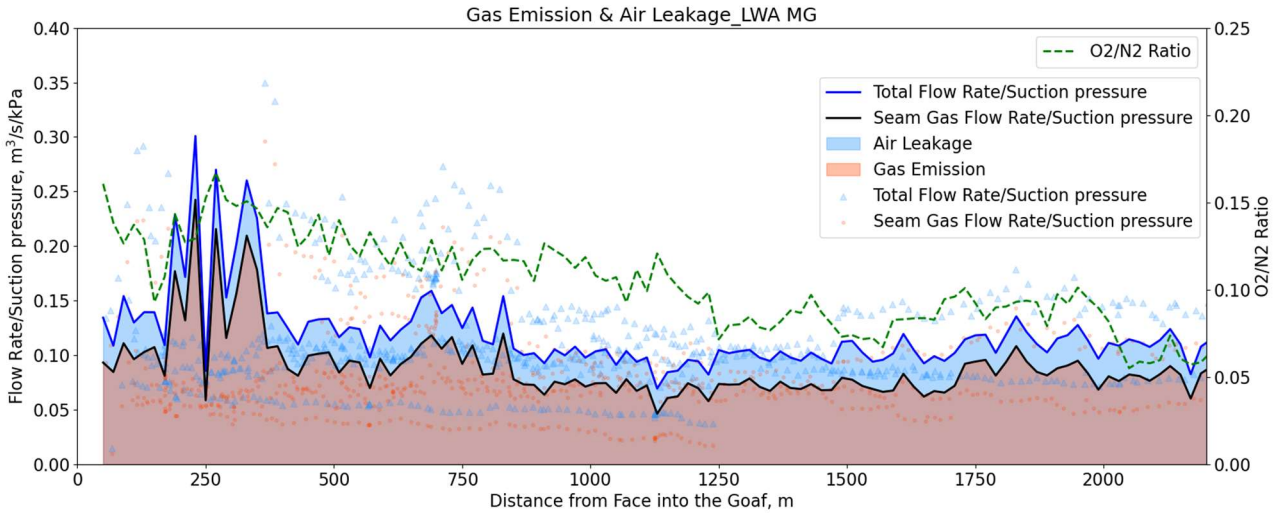

(d)

Figure 9. Total flow and seam gas flow rate profiles along the (a) TG side and (c) MG side goaf in LW A; total flow and seam gas flow rate profiles normalised by suction pressure along the (b) TG side and (d) MG side goaf in LW A

Based on the linear relationship between the suction pressure and the flow rate illustrated in Section 3.1, the flow rate values are normalised by dividing the corresponding suction pressure, as shown in Figure 9 (b). By excluding the impact of suction pressure on flow rate, the goaf natural characteristic will be the only factor controlling flow rate. The normalised total flow rate rises quickly until the peak, which is about 0.17 m^3/s/kPa, and then slowly drops to around 0.11 m^3/s/kPa at 800 m. The curve of normalised seam gas flow rate shows a similar trend, which peaks at 0.12 m^3/s/kPa and levels off at ~0.07 m^3/s/kPa. There is no significant difference in air leakage over the entire studied goaf length. Figure 9 (b) also shows the O_2/N_2 ratio decreases gradually from 0.22 to 0.08 as moving into the deep goaf along the TG side of LW A, reflecting the process of oxygen depletion and self-inertisation. Note that no nitrogen injection was conducted in the study panels.

Figure 9 (c) shows the flow rate trend at the MG side goaf of LW A is similar to that at the TG side. The total flow rate reaches its peak value of 0.6 m^3/s at 120 m. It quickly decreases to 0.4 m^3/s along with the reduction in suction pressure, and slowly decreases to about ~0.35 m^3/s at 1000 m and then levels off. The seam gas flow rate trend is also consistent with the total flow rate. Besides, the air leakage represented by the blue shaded area increases with the flow rate and suction pressure in the range of 0-120 m, after that the change of air leakage is insignificant. The normalised flow rate results by dividing suction pressure are shown in Figure 9 (d), and the flow rate trend after eliminating the suction pressure influence stays almost the same. The normalised values remain steady after 800 m from the working face: the normalised total flow rate is nearly 0.1 m^3/s/kPa and the normalised seam gas flow rate is fluctuating at about 0.075 m^3/s/kPa. Figure 9 (d) also shows no apparent change in air leakage over the whole study goaf length, but the O_2/N_2 ratio has a continuous downward trend from 0.15 to 0.05, indicating faster self-inertisation and lower risk in the MG side goaf than the TG side.

The distribution of gas emission and air leakage rate along the TG and MG sides in LW B, with respect to different face-to-hole distances, are shown in Figure 10. The horizontal and vertical axes used here are the same as the above figures for LW A. As shown in Figure 10 (a), the total flow rate of TG goafholes in LW B shows an upward trend and reaches a peak of 0.65 m^3/s at about 200 m from the face, after which it decreases to 0.45 m^3/s. Then the total flow rate rises back to 0.65 m^3/s at 400-600 m in the goaf, which is followed by a downward trend. However, as only one goafhole was operated long enough to record gas production data after 560 m, the second peak near the 600 m goaf is believed to be caused by limited monitoring results from a single goafhole. The variation of suction pressure indicated by the dotted red line is also consistent with the total flow rate change. The seam gas flow rate first rapidly increases to a peak of 0.45 m^3/s at 200 m and then decreases slowly to 0.2 m^3/s at 800

m, except for a gentle rise in 400-600 m. The air leakage at the TG side gradually increases in the 0-200 m and then continues increasing with a low rate until 600 m. After that, the air leakage rate decreases rapidly with the suction pressure decreasing. From Figure 10 (b), the normalised total flow rate varies in the range of 0.15-0.225 $m^3/s/kPa$, and the normalised gas flow rate falls in between 0.075-0.15 $m^3/s/kPa$. After dividing the suction pressure, the air leakage rate shows an overall increasing trend. The O_2/N_2 ratio drops gradually from 0.24 to 0.10 at the first 500 m as it goes deeper into the goaf. After 500 m, the O_2/N_2 ratio partially recovered to 0.15 at 600 m, which may be attributed to the same reason as the second peak of total flow rate as explained above.

Figure 10 (c) and (d) display the raw flow rate and normalised flow rate measured at the MG goafholes in LW B. B-MG01 is not shown in these figures as no flow rate data were successfully retrieved. In the range of 0-800 m behind the face, the total flow rate on the MG side slowly reduces from 0.6 m^3/s to 0.35 m^3/s, and the value of seam gas flow rate drops from 0.45 m^3/s to 0.2 m^3/s. The total flow rate and seam gas flow rate then remain stationary after 800 m. The suction pressure rises to around 3 kPa at 800 m and then maintains a constant level from 800 m to 2000 m. However, the air leakage rate does not change significantly except a minor increase after 1300 m. As shown in Figure 10 (d), the normalised total flow rate and normalised gas flow rate decrease to 0.11 $m^3/s/kPa$ and 0.075 $m^3/s/kPa$ at 800 m, respectively, and then remain constant. The O_2/N_2 ratio declines from 0.175 to 0.05 over the studied goaf range. The air leakage rate remains generally stable after removing the effect of suction pressure.

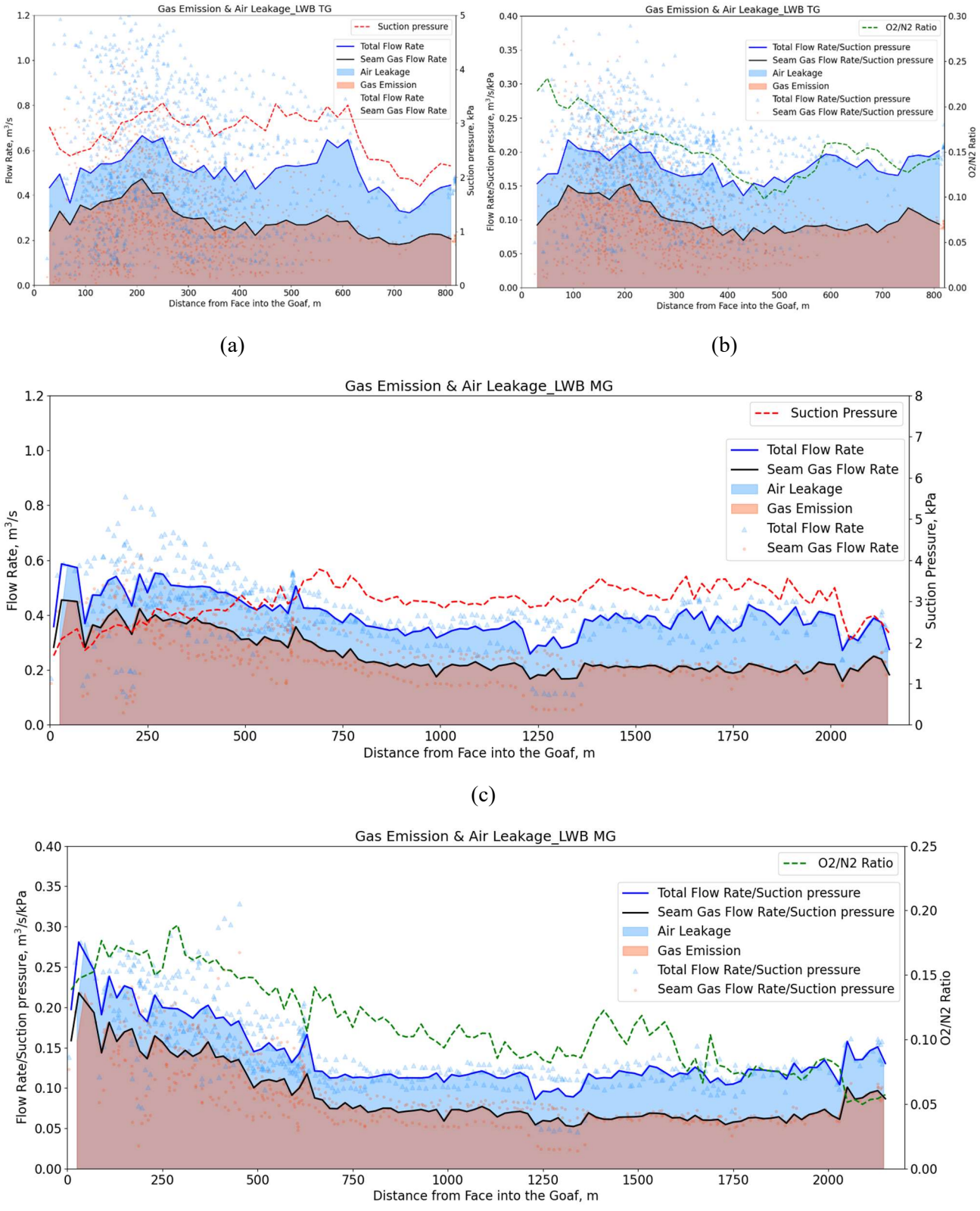

Figure 10. Total flow and seam gas flow rate profiles along the (a) TG side and (c) MG side goaf in LW B; total flow and seam gas flow rate profiles normalised by suction pressure along the (b) TG side and (d) MG side goaf in LW B

4. A THEORETICAL GOAF RESISTANCE MODEL

4.1 Theoretical Background

The goaf gas atmosphere is not only affected by the suction pressure and face-to-hole distance, but also airflow pathways. There may be multiple sources of seam gas emissions, but the air in the goaf mainly comes from the working face. After simplifying the ventilation air leakage pathways, a theoretical model to calculate goaf resistance has been proposed based on the goaf gas drainage data (suction pressure and airflow rate). Then the degree of goaf compaction and associated goaf permeability can be predicted as well.

The Hagen-Poiseuille's equation, also known as the Poiseuille equation, is suitable for the calculation of incompressible laminar fluid, and the fluid viscosity is assumed to be not affected by the flow velocity (McPherson, 2009). The Poiseuille equation can be written in the standard fluid mechanics notation (Eq. 3), which directly describes the relationship of pressure drop and volumetric flow rate. It is used for pressure drop calculation under the conditions of given pipe size and fluid viscosity in engineering applications (Figure 11).

$$\Delta P = \frac{8\mu L}{\pi r^4} Q = R_L Q \quad \text{(Eq. 3)}$$

$$R_L = \frac{8\mu L}{\pi r^4} \quad \text{(Eq. 4)}$$

where, ΔP (Pa) is the pressure drop; μ (N·s/m^2) is the fluid viscosity; L (m) is the length of the pipe; Q (m^3/s) is the volumetric flow rate; r (m) is the pipe radius; R_L (N·s/m^5) is the laminar flow resistance.

Kirchhoff's first law states that the sum of all air entering a node is equal to the sum of air leaving this node (McPherson, 2009). This law explains that the mass flow through node *j* remains constant in the ventilation network (Eq. 5). In underground ventilation, if the air density change is small and can be ignored (Eq. 6), the input flow rate for node j is equal to the output flow rate.

$$\sum_j M = \sum_j Q = 0 \quad \text{(Eq. 5)}$$

$$M = Q\rho \quad \text{(Eq. 6)}$$

where, M (kg/s) is the mass flow; ρ (kg/m^3) is the air density.

The equivalent resistance method is normally adopted in ventilation network analysis. There are usually two or more airflow pathways connected in series or parallel, and the resistance of different paths can be combined into one equivalent resistance. The schematics of ventilation airways in series

and parallel are shown in Figure 11. In the laminar flow regime, the pressure drop and flow rate have a linear relationship, and the total pressure drop of the series airways is equal to the summation of the pressure drop in each branch (Eq. 10). Finally, the equivalent resistance (Eqs. 11 or 12) of the series airways is obtained.

$$P_1 = R_1 Q \quad \text{(Eq. 7)}$$

$$P_2 = R_2 Q \quad \text{(Eq. 8)}$$

$$P_3 = R_3 Q \quad \text{(Eq. 9)}$$

$$P = P_1 + P_2 + P_3 = (R_1 + R_2 + R_3)Q \quad \text{(Eq. 10)}$$

$$R_{ser} = R_1 + R_2 + R_3 \quad \text{(Eq. 11)}$$

$$R_{ser} = \sum R \quad \text{(Eq. 12)}$$

As shown in Figure 11 (b), the total pressure drop is the same for airways in parallel. According to Kirchhoff's laws, the total flow rate through the node is equal to the sum of each branches' flow rate (Eq. 14), and the equivalent resistance of the parallel airways can be calculated (Eqs. 15 or 16).

$$P = R_1 Q_1 = R_2 Q_2 = R_3 Q_3 \quad \text{(Eq. 13)}$$

$$Q = Q_1 + Q_2 + Q_3 = P\left(\frac{1}{R_1} + \frac{1}{R_2} + \frac{1}{R_3}\right) \quad \text{(Eq. 14)}$$

$$\frac{1}{R_{par}} = \frac{1}{R_1} + \frac{1}{R_2} + \frac{1}{R_3} \quad \text{(Eq. 15)}$$

$$\frac{1}{R_{par}} = \sum \frac{1}{R} \quad \text{(Eq. 16)}$$

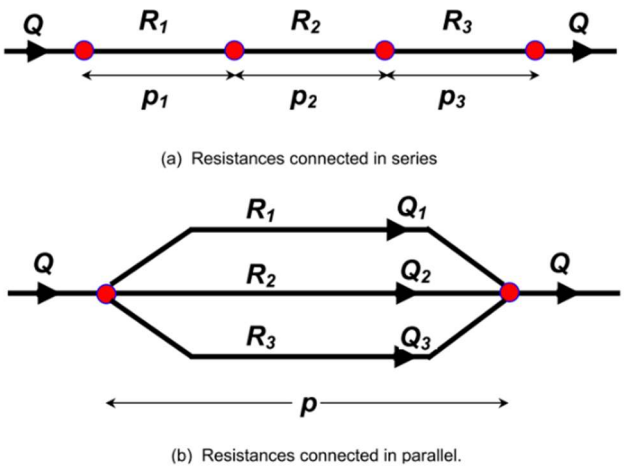

Figure 11. The combined resistances in series and parallel airways (McPherson, 2009)

4.2 Model Assumptions

To simplify the calculation of the theoretical resistance model, four assumptions are made here:

1. Air leakage can only migrate from the working face to each goafhole without any recirculation in the goaf. By applying suction pressure to the top of the goafholes, the leaked air can only flow into the slotted casing goafholes through the voids between broken rocks in the caved zone.
2. The pressure on the working face is assumed to equal the barometric pressure (i.e., 102.6 kPa based on the annual barometric data in this study mine). Then the leaked air can flow autonomously from the working face to goafholes driven by the differential pressure.
3. The airflow into each goafhole is categorised as two types of pathways: (1) the air directly leaked from the face ventilation, without being affected by other goafholes, and (2) the air migrating from the face and passing through multiple goafholes that are closer to the face. A goafhole can only receive air passing from its nearest neighbouring goafhole.
4. The air passing between neighbouring goafholes can only travel in one-direction from the face to deep goaf. In addition, the differential pressure between two neighbouring goafholes need to be positive to facilitate the migration of leaked air.
5. The air resistance in the first type of pathway is equal to the combined resistances of air flowing through the second type of pathway originated from the face.

4.3 Calculation Methods

According to the fundamental laws of fluid flow in the ventilation network and above assumptions, a series of equations were proposed to calculate the resistance of different air leakage pathways in the goaf. The resistance of each airflow branch in the goaf can be calculated after applying the field goaf gas drainage data (pressure difference and leaked airflow rate) in the resistance calculation method. To explain the proposed method, Figure 12 shows an example of a simplified ventilation network with two goafholes, where each blue arrow describes one possible airflow pathway from the face to the goafholes. As shown in the figure, each goafhole can only receive leaked air from the face directly or the neighbouring goafhole closer to the face (the one on its left in Figure 12). Note that the blue curves in this figure and the following ones only symbolise ventilation branches based on the graphic convention in mine ventilation network analysis, and they do not represent the actual air particle movement pathways in the goaf. Also, given the paper aims to develop a one-dimensional air leakage model from the face to different goafholes, the entire longwall face is simplified as a point source at

the geometry centre of the longwall. Given that air leakage can occur across the entire longwall face from the MG to TG, this assumption can be only justified for the simplified 1D model.

The following parameters can be obtained from the raw goaf drainage data: Q_1 and Q_2 (m^3/s) represent the air leakage flow rate from goafholes BH_1 and BH_2; ΔP_{01}, ΔP_{12} and ΔP_{12} (kPa) represent the pressure loss of three airflow pathways, from the working face to BH_1, the working face to BH_2, and BH_1 to BH_2, respectively. Using these known parameters, the resistance from the working face to BH_1, the working face to BH_2, and BH_1 to BH_2, as denoted by R_{01}, R_{02}, and R_{12} ($N \cdot s/m^5$), respectively, can be calculated from the equations below (Eq. 17-Eq. 22). Besides, these equations can be used to calculate Q_{01}, Q_{02} and Q_{12} (m^3/s) which refer to the air leakage flow rate of the three different paths, from the working face to BH_1, the working face to BH_2, and BH_1 to BH_2, respectively. Therefore, using the six equations below, all six unknow parameters (R_{01}, R_{02}, R_{12}, Q_{01}, Q_{02}, Q_{12}) can be solved simultaneously, given that (Q_1, Q_2, ΔP_{01}, ΔP_{02}, and ΔP_{12}) are known from goaf drainage data.

$$Q_{01} = Q_1 + Q_{12} \quad \text{(Eq. 17)}$$

$$Q_2 = Q_{12} + Q_{02} \quad \text{(Eq. 18)}$$

$$\Delta P_{01} = R_{01} Q_{01} \quad \text{(Eq. 19)}$$

$$\Delta P_{02} = R_{02} Q_{02} \quad \text{(Eq. 20)}$$

$$\Delta P_{12} = \Delta P_{02} - \Delta P_{01} = R_{12} Q_{12} \quad \text{(Eq. 21)}$$

$$R_{02} = R_{01} + R_{12} \quad \text{(Eq. 22)}$$

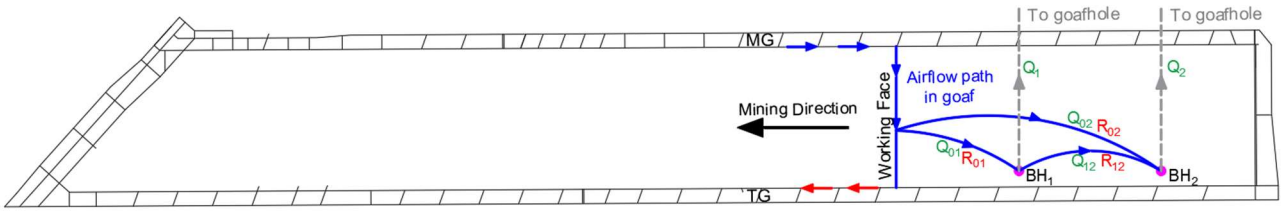

Figure 12. A schematic of the simplified goaf ventilation network (2 goafholes case)

When there are three goafholes working simultaneously (Figure 13), the first two goafholes, BH_1 and BH_2, can be combined into an equivalent goafhole $BH_{1,2}$ to simplify the calculation. Using this equivalent assumption, the required parameters of the equivalent goafhole $BH_{1,2}$ can be obtained by Eq. 23-Eq. 27 based on the assumptions in Section 4.2. Note that under the assumption of 'equivalent goafhole', Q_{23} represents all air leaking from previous boreholes to BH_3. This includes air flowing indirectly from BH_1 to BH_3 (bypassing BH_2) and directly from BH_2 to BH_3. Thus, no need to have a separate airway assumed to connect between BH_1 and BH_3, which largely simplifies the goaf ventilation network. All these parameters have the same units as the two goafholes case. Since Q_1, Q_2,

Q_3, ΔP_{01}, ΔP_{02}, ΔP_{03} are known parameters measured from each goafhole, all airway resistances (R_{01}, R_{02}, R_{03}, R_{12}, R_{23}) can be solved following the steps below.

(1) Calculate $Q_{01\text{-}EQ}$, $Q_{2\text{-}EQ}$, $\Delta P_{01\text{-}EQ}$, $\Delta P_{02\text{-}EQ}$, and $\Delta P_{12\text{-}EQ}$ using Eq. 23 to Eq. 27.

(2) Apply parameters obtained from Step (1) to Eq. 17 to Eq. 22, and thus for three active goafholes, their airway resistances ($R_{01\text{-}EQ}$, R_{03}, R_{23}) and air quantity ($Q_{01\text{-}EQ}$, Q_{03}, Q_{23}) can be calculated following the two goafholes scenario.

(3) Once $R_{01\text{-}EQ}$ is solved, then R_{02} can be solved using Eq. 29 and so as R_{01} and R_{12}.

$$Q_{01-\mathrm{EQ}} = Q_{1-EQ} + Q_{23} = Q_1 + Q_2 + Q_{23} \quad \text{(Eq. 23)}$$

$$Q_{2-EQ} = Q_3 \quad \text{(Eq. 24)}$$

$$\Delta P_{01-EQ} = \Delta P_{02} \quad \text{(Eq. 25)}$$

$$\Delta P_{02-EQ} = \Delta P_{03} \quad \text{(Eq. 26)}$$

$$\Delta P_{12-EQ} = \Delta P_{23} = \Delta P_{03} - \Delta P_{02} \quad \text{(Eq. 27)}$$

$$R_{01-EQ} = \frac{1}{\frac{1}{R_{01}+R_{12}} + \frac{1}{R_{02}}} = \frac{1}{\frac{1}{R_{02}} + \frac{1}{R_{02}}} = \frac{R_{02}}{2} \quad \text{(Eq. 28)}$$

$$R_{02} = 2R_{01-EQ} \quad \text{(Eq. 29)}$$

If ΔP_{23} is negative, based on the assumption, this indicates there is no air flowing between BH_2 and BH_3. Thus, R_{23} is assumed to be infinity large in this case, and R_{03} is equal to $\Delta P_{03}/Q_3$. The other airway resistances (R_{01}, R_{02}, R_{12}) are solved by Eq. 17 to Eq. 22, the same as the two goafholes scenario.

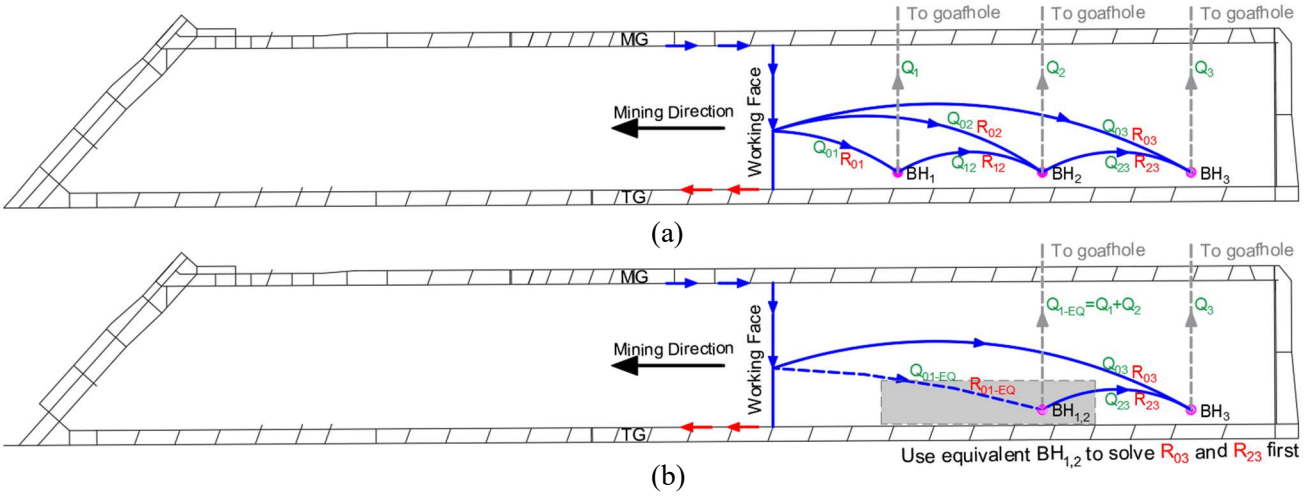

Figure 13. A schematic of the simplified goaf ventilation network (3 goafholes case) (a) Base model (b) Equivalent goafhole ($BH_{1,2}$) model

If there are n goafholes working simultaneously (n>3), the first (n-1) goafholes can be combined into a new equivalent goafhole to simplify the calculation as shown in Figure 14 (a) and (b). The relevant parameters of the new equivalent goafhole $BH_{1,n-1}$ can be calculated using Eq. 30-Eq. 34, and then follow the two goafholes case using Eq. 17-Eq. 22 to solve $R_{01\text{-}EQ}$, $R_{0,n}$, and $R_{n-1,n}$. If $\Delta P_{n-1,n}$ is negative, there is no air leakage between BH_{n-1} and BH_n. Therefore, $R_{n-1,n}$ is assumed to be infinity large, and $R_{0,n}$ is equal to $\Delta P_{0,n}/Q_n$.

$$Q_{01-\mathrm{EQ}} = Q_{1-EQ} + Q_{n-1,n} = \sum_{1}^{n-1} Q_i + Q_{n-1,n} \quad \text{(Eq. 30)}$$

$$Q_{2-EQ} = Q_n \quad \text{(Eq. 31)}$$

$$\Delta P_{01-EQ} = \Delta P_{0,n-1} \quad \text{(Eq. 32)}$$

$$\Delta P_{02-EQ} = \Delta P_{0,n} \quad \text{(Eq. 33)}$$

$$\Delta P_{12-EQ} = \Delta P_{n-1,n} = \Delta P_{0,n} - \Delta P_{0,n-1} \quad \text{(Eq. 34)}$$

Once $R_{0,n}$ and $R_{n-1,n}$ are determined, the same equivalent goafhole assumption can be repeated by merging the first (n-2) goafholes into a new equivalent goafhole $BH_{1,n-2}$ (Figure 14 (c)), then $R_{0,n-1}$ and $R_{n-2,n-1}$ can be calculated by repeating the previous steps. Thus, by back-propagating from BH_n to BH_2 after applying equivalent goafhole assumption and Eq. 17 to Eq. 22 multiple times, for n active goafholes, their airway resistances can be calculated one by one. For a single goafhole BH_n, $R_{0,n}$ represents the goaf resistance for air migrating from the working face to the goafhole, which is the air leakage resistance in the first type of pathway as introduced in Section 4.2.

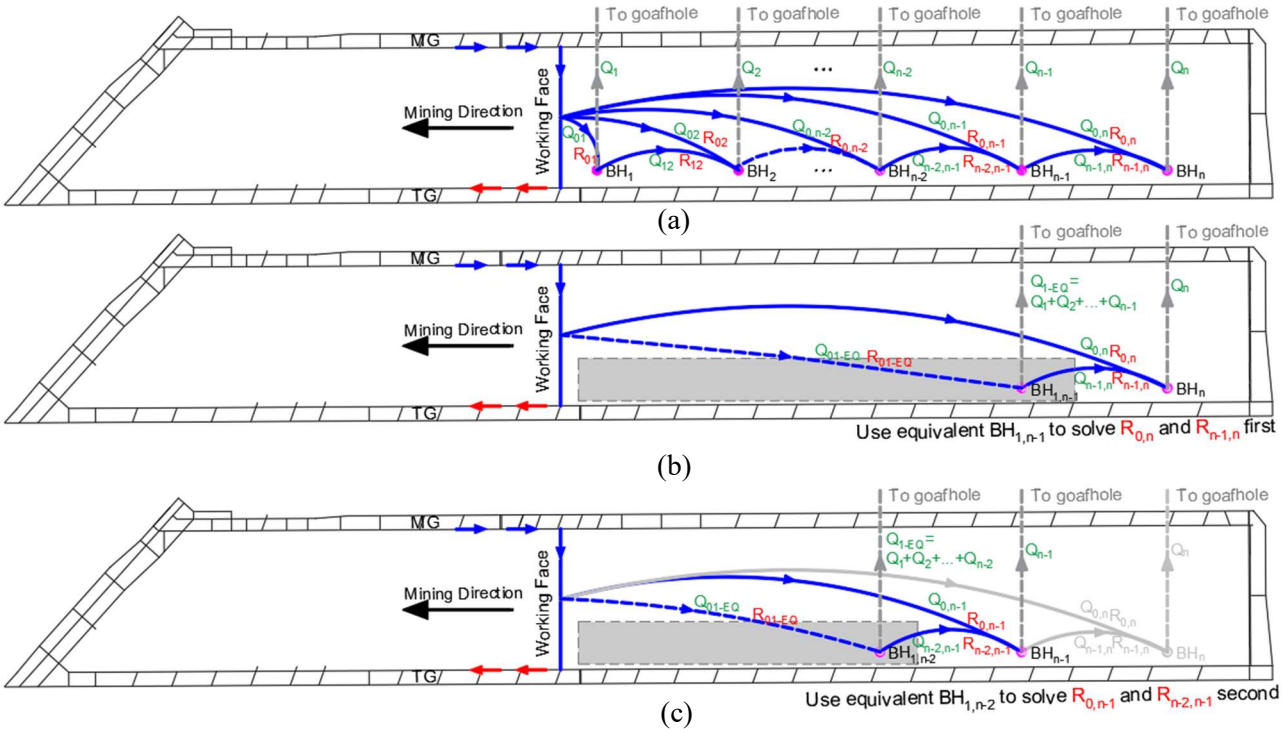

Figure 14. A schematic of the simplified goaf ventilation network (n goafholes case) (a) Base model (b) Equivalent goafhole ($BH_{1,n-1}$) model (c) Equivalent goafhole ($BH_{1,n-2}$) model

4.4 Results Analysis

Based on the above theoretical resistance model (3 goafholes case: Eqs 17 to 29) and goaf gas drainage field data, the calculated resistance (R_{01}, R_{02}, and R_{03}) is presented in Table 1, which refers to the air migration from the working face to the bottom of three simultaneously working goafholes (BH_1, BH_2, and BH_3), respectively. It will not be affected by any other active goafholes that are closer to the face. The pressure differences in Table 1 were calculated after considering different types of pressure loss of the leaked air in goafholes. Based on the air leakage flow rates extracted from goafholes, the Reynolds number (Re) in goafholes can be evaluated, thus determining that the flow in goafholes is fully turbulent, despite the air migration in the goaf follows laminar flow assumption (see Section 3.1). Indeed, a small transition flow area would present at the bottom of goafholes, but it is not considered in the research due to its small size and limited impact.

Table 1. Resistance from the working face to example goafholes (3 goafholes case)

Operating goafholes name	**A-TG03 (BH_1)**	**A-TG02 (BH_2)**	**A-TG01 (BH_3)**
Distance to the working face (m)	20.94	73.82	134.26
Suction pressure (kPa)	-1.514	-1.810	-2.813
Head pressure loss (ΔP_{col} ,kPa)	0.926	0.926	0.926
Friction pressure loss (ΔP_{fric} ,kPa)	0.026	0.013	0.029
Local pressure loss (ΔP_{local} ,kPa)	0.002	0.001	0.002
Pressure difference between the working face and goafholes (ΔP_{01}, ΔP_{02}, ΔP_{03}, kPa)	-0.560	-0.870	-1.856
Air leakage rate (Q_1, Q_2, Q_3, m^3/s)	0.122	0.084	0.123
Resistance from the working face to goafholes (R_{01}, R_{02}, R_{03} , $\times 10^6$ $N \cdot s/m^5$)	0.003	0.007	0.025
Cumulative air leakage rate (m^3/s)	0.329	0.207	0.123
Permeability (m^2)	1.542×10^{-7}	2.198×10^{-7}	1.110×10^{-7}

For the turbulent pipe flow in goafholes, the head pressure loss (Eq. 35) is the same for all vertical goafholes when assuming the goafholes depths at different locations are the same. Moreover, the pressure loss due to viscous effects can be calculated by the Darcy–Weisbach equation for turbulent flow (Eq. 36). For the air leakage transport from the goaf to goafholes with narrow diameters, the local pressure loss can be estimated by Eq. 38.

$$\Delta P_{col} = \rho g \Delta h \quad \text{(Eq. 35)}$$

where, ΔP_{col} (Pa) is head pressure loss; ρ (kg/m^3) is the fluid density, equal to 1.18 (kg/m^3) for the leaked air at 26 ℃; g (m/s^2) is the local acceleration due to gravity; Δh (m) is the column height of the fluid (goafhole depth).

$$\Delta P_{fric} = f_D \frac{\rho v^2 L}{2D} \quad \text{(Eq. 36)}$$

where, ΔP_{fric} (Pa) is friction pressure loss in pipes; f_D is the Darcy friction factor (also called flow friction coefficient), equal to 0.0242 based on the Colebrook Equation (Eq. 37) for the average leaked air turbulent flow (~0.2 m^3/s) in goafholes; v (m/s) is the mean flow velocity, experimentally measured as the volumetric flow rate; L (m) is the length of the flow; D (m) is the hydraulic diameter of the goafhole.

$$\frac{1}{\sqrt{f_D}} = -2log\left[\frac{2.51}{Re\sqrt{f_D}} + \frac{\epsilon}{3.7D}\right] \quad \text{(Eq. 37)}$$

where, ϵ (m) is the roughness of the goafhole surface, equal to 0.3×10^{-3} m; Re is the Reynolds number, can be calculated by Eq.1; μ (N·s/m^2) is the fluid viscosity, which is assumed as a constant value of

1.84×10^{-5} N·s/m^2 for the leaked air at 26 °C. Considering the normal goaf temperature is around 40 °C and the short residual time of leaked air in the goaf, the impact of temperature change on viscosity (1.92×10^{-5} N·s/m^2 at 40 °C) would only has marginal impact on the results, which is ignored here.

$$\Delta P_{local} = K_r \frac{\rho v^2}{2} \quad \text{(Eq. 38)}$$

where, ΔP_{local} (Pa) is local pressure loss in pipes; K_r is the local flow coefficient, equal to 0.5, leaked air flow from the goaf caved zone into narrow goafholes (Stewart, 2016).

Similar to the previous example of the three goafholes case, it is possible to calculate the leaked air resistance from the working face to different operating goafhole locations for each day of the LW A over its entire operating duration, and it will not be affected by any other active goafholes that are closer to the face. As a result, the resistance change along the TG and MG side goaf in Figure 15 can be obtained. The face-to-hole distance analysed on the TG side is 0-500 m, and the range on the MG side is 0-2000 m. Since fewer data points outside these ranges will affect the moving average trend, they are not used in calculating the resistance and permeability results. In Figure 15, the goaf resistance calculated from some example goafholes is represented by the scatter points in different colours. In general, at both the TG and MG side goaf, the farther away from the working face, the greater the goaf resistance. As the resistance of airflow pathways in the goaf increases with an increase of the face-to-hole distance, it is more difficult for deep goafholes to draw oxygen from the working face, and this will also affect gas drainage efficiency as goafholes need to work harder (more suction) to capture the same amount of gas as before. Based on the above goaf resistance calculation results, the amount of ventilation air contamination in each goafhole can be predicted at a given suction pressure.

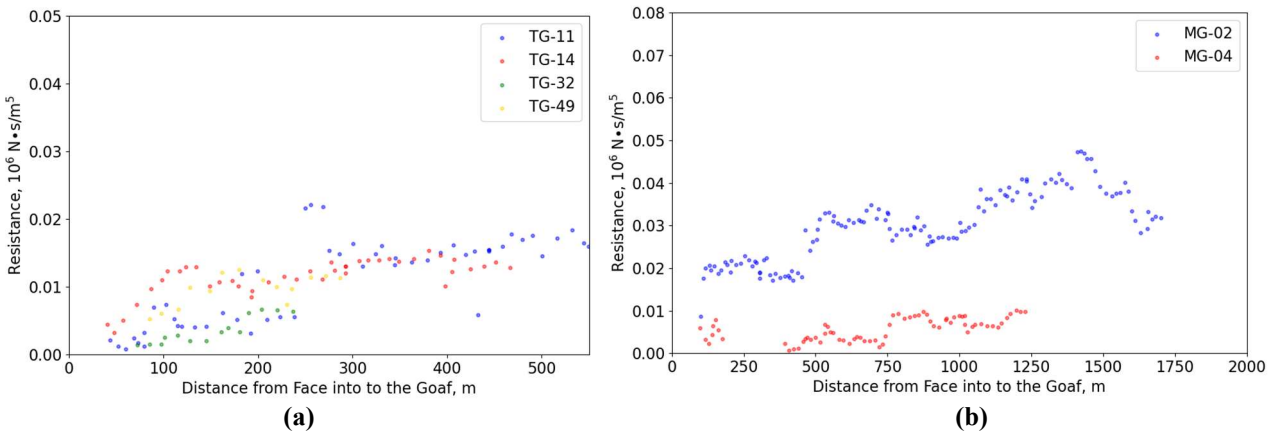

Figure 15. Goaf resistance profiles calculated on selected goafholes along the (a) TG side and (b) MG side goaf at LW A

As shown in Figure 16, the calculated resistance for all goafholes in LW A are represented by blue triangles. To smooth the scatter plots, the blue triangles were rolling-averaged per 10 m at the TG side to obtain the resistance trend (as denoted by the solid blue line). The resistance trend can also be obtained along the MG side goaf, using a 20 m interval for the rolling average. In Figure 16 (a), the goaf resistance at the TG side of LW A increases rapidly first, reaches a peak of 0.02×10^6 N·s/m^5 at about 100 m, and then remains stable till 500 m from the working face. The goaf resistance trend on the MG side (Figure 16 (b)) is similar to that of the TG side, which rapidly rises to the peak value of 0.03×10^6 N·s/m^5 in the initial 200 m, and then fluctuates after 200 m. The MG side data points in Figure 16 (b) are sparse due to the small number of goafholes working simultaneously at a large face-to-hole distance, which may not be statistically representative.

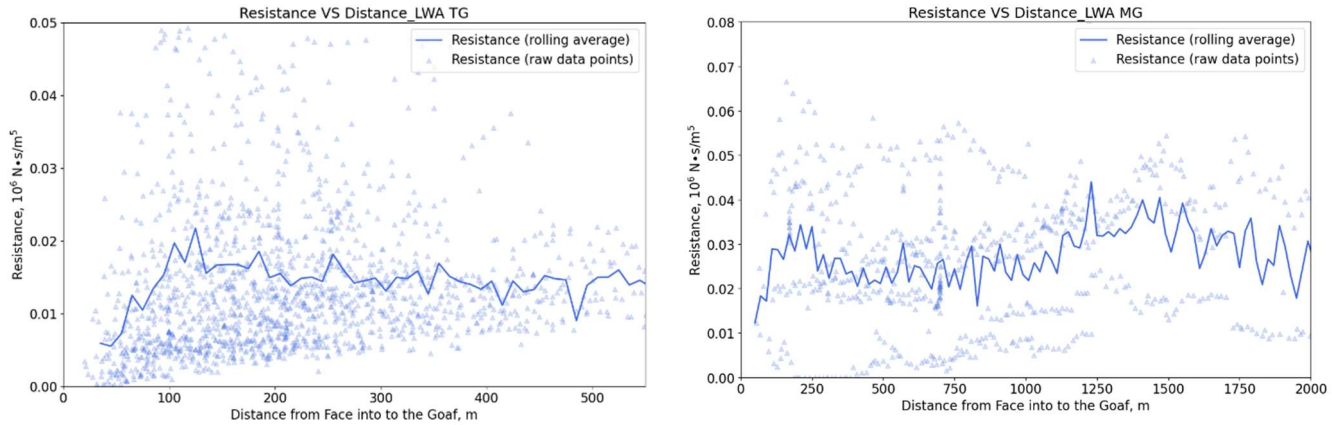

(a) (b)

Figure 16. Resistance profiles along the (a) TG side and (b) MG side goaf at LW A

5. DISCUSSIONS

5.1 Dynamic Control of Suction Pressure

The total flow rate, seam gas flow, and air leakage changes with respect to the suction pressure and the face-to-hole distance have been presented in Sections 3.1 and 3.2. Based on these goaf production data analysis results in LW A and LW B, the instant control strategy to optimise goaf gas drainage while minimising spontaneous combustion/gas explosion risks could be proposed. This strategy is through adjusting the suction pressure to control gas drainage valves, which can maintain the gas emission and air leakage in captured goaf gas in a normal range. To be more specific, goaf gas drainage control strategies will be divided into two scenarios: the working face nearby zone and the deep goaf zone.

The total drainage flow rate reaches its maximum at 100-200 m behind the working face at LW A and LW B (Figures 9 and 10). Over this zone, the flow rate increase is mainly due to the high suction

pressure applied. Depending on the specific gas emissions at the study mine, this high suction pressure may result in more air leakage from the face and more seam gas being captured. When the goafhole is too close to the working face, it is more likely to connect with the ventilation system and draw a large amount of O_2 to enter the goaf in a short time. Although the priority of goafholes close to the face is to maintain a low CH_4 concentration in the tailgate return, high suction pressure should be applied with caution for these goafholes, especially when the specific gas emissions are low. It is necessary to closely monitor the gas trends in the goaf to detect excessive air ingress. After removing the impact of the suction pressure change, methane purity increases gradually as moving into the 100-200 m face-to-hole distance. In contrast, the air content remains almost unchanged in this zone, but the O_2 proportion decreases continuously, suggesting O_2 has been consumed by slow oxidation.

As the air leakage was increased with high suction pressure, it is suggested to reduce the suction pressure to minimise O_2 migration into the goaf. With the face-to-hole distance increases, an inert goaf atmosphere has been gradually developed by removing less seam gas in the deep goaf zone, indicating low spontaneous combustion risks. If the O_2 concentration did not reach the trigger value in the Trigger Action Response Plans (Xiang et al., 2021), a relatively high suction force was still applied for deep goafholes as they are far from the ventilation air. Thus, it has a higher chance to capture high-purity seam gas. Besides, maintaining a strong suction in these deep goafholes can create a low-pressure environment that pulls back newly released gas away from the face. O_2 level and O_2/N_2 ratio also need to be monitored closely from the TG goafholes in deep goaf in order to prevent air leakage from goaf seals after imposing strong suction pressure.

5.2 Applications of the Theoretical Resistance Model

The theoretical resistance model can predict the compaction degree of collapsed rocks and the permeability distribution in the goaf. As Figure 16 shows, the goaf resistance increases along with the face-to-hole distance firstly and then becomes stable. Since resistance has an inverse relationship with permeability, it can be used to predict that the permeability trend in the goaf was continually decreased until it reached the lowest value and remained unchanged, which is constant with other goaf permeability distribution studies (Szlazak, 2001; Szlazak and Szlazak, 2001; Marts et al., 2014; Zhang et al., 2016). At the same time, these results can be applied to predict the degree of compaction of the overlying strata. Due to the hydraulic supporting near the working face, the upper strata of the longwall panel do not collapse excessively near the working face, and the permeability of this area is high. The roof strata gradually collapse with the increasing face-to-hole distance in the goaf, and the voids

between crushed rocks in the goaf are gradually squeezed until fully compacted. A quantitative estimation of goaf permeability based on the goaf resistance calculation results will be attempted below.

From the theoretical resistance model results, the resistance (R_{01}, R_{02}, R_{03}, …, R_{0n}) from the working face to each goafhole (BH_1, BH_2, BH_3, …, BH_n) can be calculated, and then the relevant 'pipe radius' (r_1, r_2, r_3, …, r_n) were solved by Eq. 4. Moreover, the 'length of the pipe' (L in Eq. 4) in the permeability calculation means the face-to-hole distance. In this way, the permeability can be calculated by the following Eq. 27. In this equation, the height of the cross-sectional area (A in Eq. 27) is assumed as a constant value of 10 m, which is roughly three times the mining height of the target coal seam. The width of the cross-sectional area depends on the number of simultaneously working goafholes (n), which equals $2\sum_{i=1}^{n} r_i$ in Figure 17. Furthermore, the pressure drop (ΔP in Eq. 27) refers to the differential pressure between the working face and each goafhole location, which is calculated based on the given suction pressure at the goafhole top surface and various types of pressure losses (Eqs. 35 to 38). The volumetric flow rate (Q in Eq. 27) is the cumulative value of air leakage rate in all outby goafholes that are operating simultaneously on a same date at a specific goafhole location. As a result, the cumulative air leakage rate for permeability calculation and the corresponding results for three TG side goafholes of LW A operating on the same day are also shown in Table 1. Figure 18 displays the cumulative air leakage rate raw data points and rolling average trend along the TG side of LW A.

$$Q = \frac{kA\Delta P}{\mu L} \qquad \text{(Eq. 27)}$$

where, Q (m^3/s) is the volumetric flow rate; k (m^2) is the permeability; A (m^2) is the cross-sectional area; ΔP (Pa) is the pressure drop; μ $(N \cdot s/m^2)$ is the leaked air viscosity, which is 1.84×10^{-5} $N \cdot s/m^2$ at 26 ℃; L (m) is the length of the flow path.

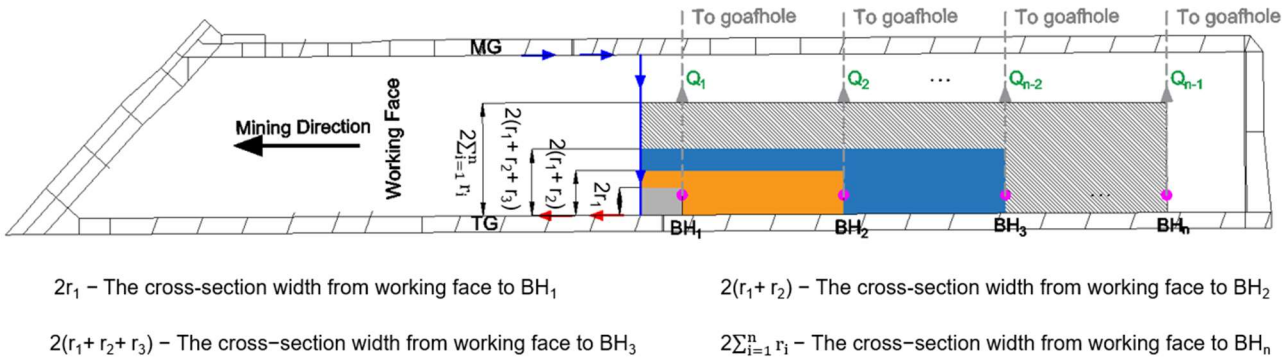

Figure 17. A schematic of the simplified goaf air leakage area (n goafholes case)

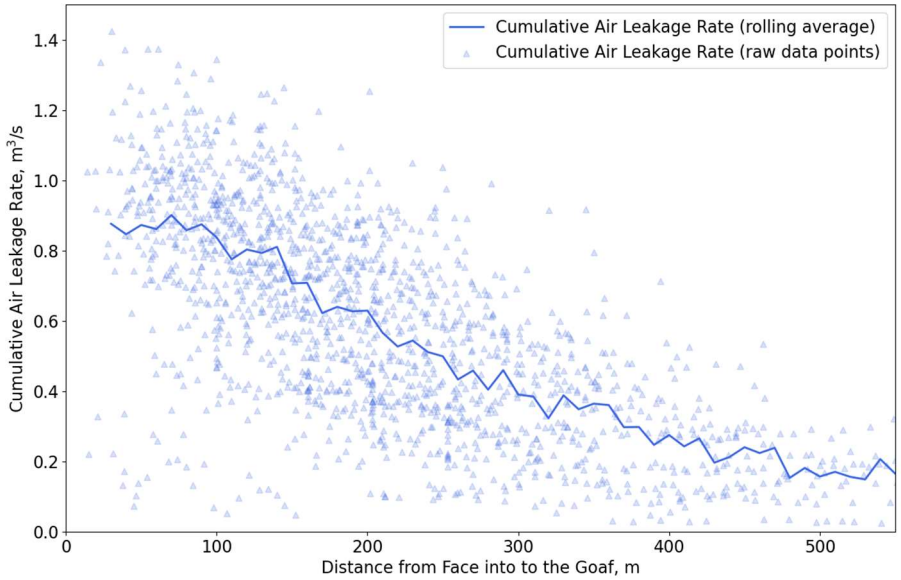

Figure 18. Cumulative air leakage rate profiles along the TG side goaf at LW A

As shown in Figure 19, the predicted permeability values for all TG side goafholes in LW A throughout the whole mining operation are depicted by blue triangles. These permeability data points were averaged per 10 m to determine the rolling average trend with respect to the face-to-hole distance (the solid blue line). The average permeability followed the declining trend along the TG side goaf, rapidly decreasing from ~1.1×10^{-6} m^2 to ~0.3×10^{-6} m^2 at the first 100 m and then maintaining stable afterwards.

Although on-site measurement of goaf permeability (e.g., packer test) may provide more direct and accurate results, it cannot be widely implemented due to high implementation costs. In addition, the dynamic longwall coal extraction process normally results in the variation of goaf permeability throughout the longwall life cycle, which cannot be rapidly determined using on-site measurement. As an alternative method, the calculated permeability based on this theoretical resistance model is in a reasonable range, which is also consistent with the goaf permeability distribution results (10^{-9} m^2 to 10^{-5} m^2) obtained in previous geomechanical models (Esterhuizen and Karacan, 2005, 2007; Karacan, 2009a; Ren et al., 2011; Marts et al., 2014; Zhang et al., 2016; Zhang et al., 2019). Moreover, the theoretical model utilises the readily available goaf gas production data, which could provide a rapid and first-hand estimation of goaf permeability distribution. The calculated goaf permeability can be used as an input in subsequent goaf CFD models.

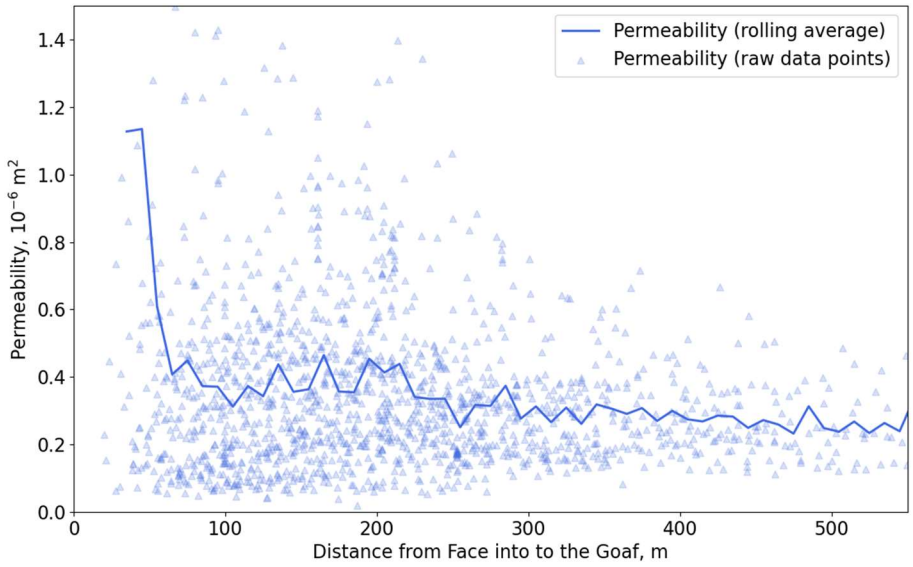

Figure 19. Permeability profiles along the TG side goaf at LW A

5.3 Limitations of the Theoretical Resistance Model

However, this theoretical resistance model may also have some drawbacks. This theoretical resistance model is built on the assumption that all airflows in the goaf are laminar flows. The laminar flow assumption is based on the fact that most of the raw data points in Figure 5 followed the positive linear relationship between the suction pressure and flow rate. After dividing the total flow rate by the suction pressure to achieve normalization, the goaf gas flow is found to be not completely laminar in the first 300 m (Figure 9). As the goaf gas drainage data used in this theoretical model are only collected from defined goaf locations (TG and MG goafholes that are aligned linearly in the goaf), this theoretical model could be improved under different types of flow assumptions.

This model assumed that the leaked air migration could only occur from the working face to each goafhole and between adjacent goafholes to simplify airflow pathways in the goaf caved zone. Figure 20 shows that the total leaked air ($Q_{n,t}$) extracted from the goafhole BH_n may contain not only $Q_{n,c}$ through the caved zone but also a small amount ($Q_{n,f}$) through fractures in the fractured zone and flow into the BH_n with the slotted casing. The ratio of $Q_{n,c}$ to $Q_{n,f}$ can be assumed as $r_{c,f}$. In our previous assumptions, to simplify the above theoretical resistance model and permeability calculations, the effect of air leakage from the fractured zone was ignored, and thus $Q_{n,t}$ was the same as $Q_{n,c}$. However, to understand the impact of $Q_{n,f}$ when it is non-trivial, this section assumes $r_{c,f}$ can vary from 2 to 50. Therefore, as shown in Figure 20, $R_{n,f}$:$R_{n,c}$:$R_{n,t}$ would equal to $r_{c,f}$:1:[$r_{c,f}$/(1+ $r_{c,f}$)] if the fraction of $Q_{n,f}$:$Q_{n,c}$:$Q_{n,t}$ is 1:$r_{c,f}$:(1+ $r_{c,f}$) based on the law of combined resistances in parallel airways (Eqs 13 to 16). As a result, the permeability change along the TG side of LW A is shown in Figure 21 with different $r_{c,f}$ values. According to Figure 21, adjusting $r_{c,f}$ values have limited impact on permeability,

and the smaller $r_{c,f}$, the lower the permeability. However, it is also reported from the site that goafholes can be blocked or sheared off during the longwall retreat, which will largely increase their overall resistance. This is not considered in this research due to the large uncertainty of goafhole blockage. Therefore, if a server blockage occurs in that goafhole, the calculated goaf resistance may also contain a portion of goafhole resistance.

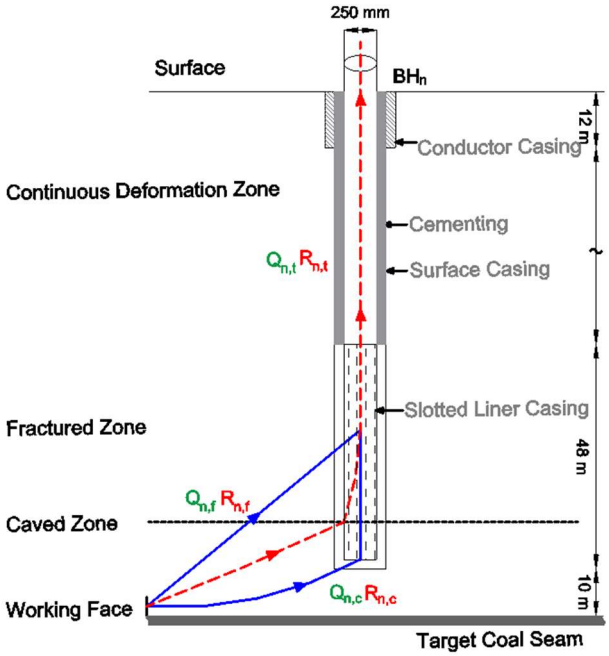

Figure 20. Cross-section of potential air leakage pathways from the working face to an example goafhole BH_n in the case study mine (modified from Si and Belle, 2019)

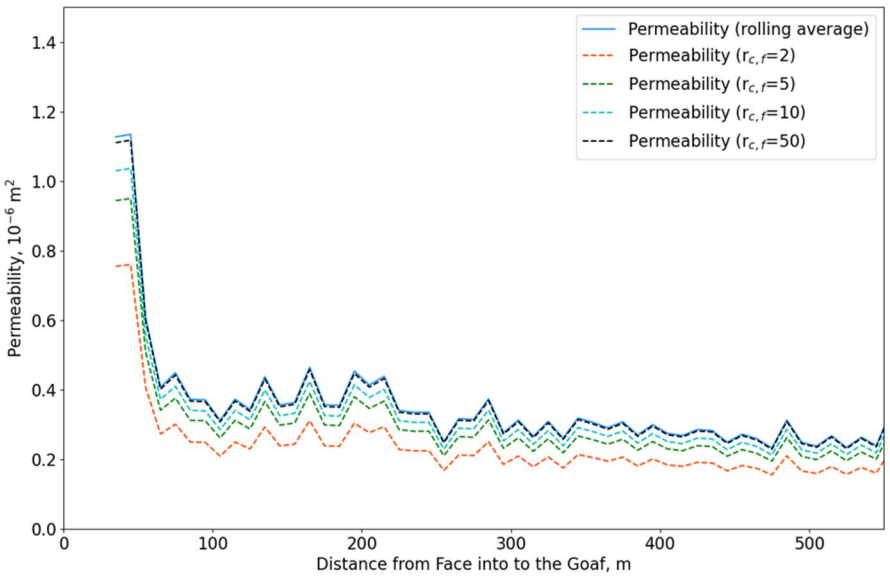

Figure 21. Permeability profiles along the TG side goaf at LW A with different $r_{c,f}$ values

Moreover, the assumption that the working face pressure is roughly equal to the barometric pressure is proposed in Section 4.2. However, the actual working face pressure is lower than the barometric pressure due to the general suction of mine body ventilation. In this theoretical resistance model, the depths of the goafholes bottom to the target coal seam are assumed to be the same at different locations, although there are slight variations in their depths depending on the surface topographic conditions. The different depths of goafholes would also cause the buoyancy effect, and the 3D air migration in the goaf or across multiple goafholes was not considered in this one-dimensional theoretical resistance model. The airflow between two adjacent goafholes can only move from the higher pressure to the lower pressure regime, and thus there are some conditions in which no flow exists between two adjacent goafholes, resulting in infinite large resistance.

6. CONCLUSIONS

This research focuses on analysing goaf gas production data from hundreds of vertical goafholes in two case study longwall panels in Australia. To evaluate goaf gas drainage effectiveness, the correlation between suction pressure, total flow rate, seam gas flow rate and air leakage rate was analysed in detail as the face-to-hole distance increases. In general, the total flow rate at the TG and MG sides has a similar trend. They both increase rapidly to the peak value at roughly the same distance, about 100-250 m into the goaf, and then slowly decrease and level off eventually. In addition, the suction pressure is found to be positively correlated with the total flow rate. As the suction pressure increases, goaf gas capture and air leakage increase. According to the effect of suction pressure on total flow rate, instant strategies for goaf gas drainage control by adjusting the suction pressure of goafholes can be implemented.

This paper also proposed a theoretical model to calculate the goaf resistance of ventilation air leakage pathways under the effect of intensive goaf drainage. The model results suggested that the resistance of air leakage pathways from the working face to individual goafholes increased with the face-to-hole distance. This resistance model can also be used to infer the permeability of the goaf caved zone, and the results are consistent with the trends and magnitudes reported in previous studies on goaf permeability. In addition, a large amount of field data was analysed in this study, and the proposed resistance model and results based on goaf gas drainage data can contribute to evaluating the goaf compaction degree and identifying high air leakage zones in the goaf, which is difficult and expensive to measure in the field. This will help mine sites to apply engineering controls (e.g., nitrogen injection, polymer plugs and temperature stoppings) to reduce air leakage into the goaf, and consequently

minimise the explosion zone size and spontaneous combustion risk. Furthermore, the calculated goaf resistance and permeability results may be used as input for other numerical models, such as CFD or Ventsim with a clear understanding of limitations, to provide field data for model calibration and validation. By combining this theoretical model results with the strengths of CFD modelling, advancement in understanding the complex goaf compaction, ventilation dynamics, airflow patterns and gas atmosphere can be made. This will be another major step towards revealing the 'inaccessible' longwall goaf behaviours during resource extraction.

ACKNOWLEDGEMENT

The authors would like to thank Australian Coal Research Association Project (ACARP) C29017 for sponsoring this research.

REFERENCES

Akgun, F. and Essenhigh, R., 2001. Self-ignition characteristics of coal stockpiles: theoretical prediction from a two-dimensional unsteady-state model. Fuel, 80(3), pp.409-415.

Borunda, A., 2019. Methane facts and information, National Geographic.

Chen, D., Pan, Z., Shi, J.Q., Si, G., Ye, Z. and Zhang, J., 2016. A novel approach for modelling coal permeability during transition from elastic to post-failure state using a modified logistic growth function. International Journal of Coal Geology, 163, pp.132-139.

Cheng, W., Hu, X., Xie, J. and Zhao, Y., 2017. An intelligent gel designed to control the spontaneous combustion of coal: Fire prevention and extinguishing properties. Fuel, 210, pp.826-835.

Coward, H. and Jones, G., 1952. Limits of flammability of gases and vapors, Washington U.S. Gov. Print. Off.

Diamond, W.P., 1995. The influence of gob gas venthole location on methane drainage: a case study in the Lower Kittanning coalbed, PA. In: Proceedings 7th US Mine Ventilation Symposium, Kentucky, USA, 5–7, Jun.

Diamond, W.P., Jeran, P.W., Trevits, M.A., 1994. Evaluation of Alternative Placement of Longwall Goaf Gas Vent Holes for Optimum Performance. USBM Report of Investigation No 9500

Duan, Y., Shen, Y., Canbulat, I., Luo, X. and Si, G., 2021. Classification of clustered microseismic events in a coal mine using machine learning. Journal of Rock Mechanics and Geotechnical Engineering, 13(6), pp.1256-1273.

Esterhuizen, E., Mark, C. and Murphy, M. M., 2010. Numerical Model Calibration for Simulating Coal Pillars, Gob and Overburden Response. Proceedings of the 29th International Conference on Ground Control in Mining. Morgantown, West Virginia, 46-57.

Esterhuizen, G.S. and Karacan, C.Ö., 2005. Development of Numerical Models to Investigate Permeability Changes and Gas Emission around Longwall Mining Panel. In: Alaska Rocks 2005, The 40th US Symposium on Rock.

Esterhuizen, G.S. and Karacan, C.Ö., 2007. A Methodology for Determining Gob Permeability Distributions and its Application to Reservoir Modeling of Coal Mine Longwalls. 2007 SME Annual Meeting. Denver, CO.

Gao, J. and Wang, H., 2010. Influence of permeability distribution on airflow field of leakage in gob, China Safety Science Journal, 30(3), pp.81–85.

Gao J., Li X., and Cui Y., 2013. Numerical simulation for airflow and gas distribution regulation in the goaf of mechanized working face, Journal of Safety and Environment, 13(2), pp.164-168.

Guo, H., Yuan, L., Shen, B., Qu, Q. and Xue, J., 2012. Mining-induced strata stress changes, fractures and gas flow dynamics in multi-seam longwall mining. International Journal of Rock Mechanics and Mining Sciences, 54, pp.129-139.

He, X., Zhang, R., Pei, X., Sun, Y., Tong, B. and Huang, H., 2008. Numerical simulation for determining three zones in the goaf at a fully mechanized coal face. Journal of China University of Mining and Technology, 18(2), pp.199-203.

Karacan, C.Ö., 2009a. Prediction of Porosity and Permeability of Caved Zone in Longwall Gobs, Transport in Porous Media, 82(2), pp.413–439.

Karacan, C.Ö., 2009b. Reconciling longwall gob gas reservoirs and venthole production performances using multiple rate drawdown well test analysis, International Journal of Coal Geology, 80(3-4), pp.181–195.

Karacan, C.Ö., 2015. Analysis of gob gas venthole production performances for strata gas control in longwall mining', International Journal of Rock Mechanics and Mining Sciences, 79, pp.9–18.

Karacan, C.Ö., Diamond, W.P., Schatzel, S.J. and Garcia, F., 2006. Development and Application of Reservoir Models for the Evaluation and Optimization of Longwall Methane Control Systems. National Institute for Occupational Safety and Health, Pittsburgh Research Laboratory.

Karacan, C.Ö., Esterhuizen, G.S., Schatzel, S.J. and Diamond, W.P., 2007. Reservoir simulation-based modeling for characterizing longwall methane emissions and gob gas venthole production, International Journal of Coal Geology, 71(2-3), pp.225–245.

Karacan, C.Ö., Ruiz, F.A., Cotè, M. and Phipps, S., 2011. Coal mine methane: A review of capture and utilization practices with benefits to mining safety and to greenhouse gas reduction, International Journal of Coal Geology, 86(2-3), pp.121–156.

Liu, A., Liu, S., Wang, G. and Elsworth, D., 2020. Continuous Compaction and Permeability Evolution in Longwall Gob Materials, Rock Mechanics and Rock Engineering, 53(12), pp.5489–5510.

Marts, J. A., Gilmore, R. C., Brune, J. F., Bogin Jr, G. E., Grubb, J. W., and Saki, S., 2014. Dynamic gob response and reservoir properties for active longwall coal mines, Mining Engineering, 66(12), pp.59-66.

Mcpherson, M.J., 2009. Subsurface ventilation and environmental engineering, Chapman & Hall, London; New York.

Ren, T.X. and Edwards, J.S., 2002. Goaf gas modelling techniques to maximise methane capture from surface gob wells. In: Proceedings of The 9th North American/US Mine Ventilation Symposium. Kingston, Ontario, Canada, pp.8–12 (June).

Ren, T.X., Balusu, R., and Claassen, C., 2011. Computational fluid dynamics modelling of gas flow dynamics in large longwall goaf areas.

Schmal, D., Duyzer, J. and van Heuven, J., 1985. A model for the spontaneous heating of coal. Fuel, 64(7), pp.963-972.

Si, G. and Belle, B. 2019, Performance analysis of vertical goaf gas drainage holes using gas indicators in Australian coal mines. International Journal of Coal Geology, 216, p.103301.

Si, G., Jamnikar, S., Lazar, J., Shi, J.Q., Durucan, S., Korre, A. and Zavšek, S., 2015a. Monitoring and modelling of gas dynamics in multi-level longwall top coal caving of ultra-thick coal seams, part I: Borehole measurements and a conceptual model for gas emission zones. International Journal of Coal Geology, 144–145, pp.98–110.

Si, G., Shi, J.Q., Durucan, S., Korre, A., Lazar, J., Jamnikar, S. and Zavšek, S. 2015b, Monitoring and modelling of gas dynamics in multi-level longwall top coal caving of ultra-thick coal seams, Part II: Numerical modelling. International Journal of Coal Geology, 144–145, pp.58–70.

Stewart, M. 2016, Surface production operations. Volume III, Facility piping and pipeline systems. Waltham, Ma, Usa ; Kidlington, Oxford, Uk Gulf Professional Publishing Is An Imprint Of Elsevier.

Szlazak J., 2001. The determination of a co-efficient of longwall gob permeability. Archives of Mining Sciences, vol. 64, No. 4, pp. 451-468

Szlazak J. and Szlazak N., 2001. Permeability of longwall gob. Proceedings of the 7th International Mine Ventilation Congress: June 17-22, 2001, Cracow, ed. Stanislaw Wasilewski, pp. 623-629.

United States Environmental Protection Agency 2019, Global Non-CO_2 Greenhouse Gas Emission Projections & Mitigation, www.epa.gov.

Wang, C., Si, G., Zhang, C., Cao, A. and Canbulat, I., 2021. Location error based seismic cluster analysis and its application to burst damage assessment in underground coal mines. International Journal of Rock Mechanics and Mining Sciences, 143, p.104784.

Wendt, M. & Balusu, R. 2002, CFD modelling of longwall goaf gas flow dynamics. Coal and Safety.

White, F.M., 2017. Fluid mechanics. New Delhi, India: Mcgraw-Hill Education.

Whittles, D.N., Lowndes, I.S., Kingman, S.W., Yates, C. and Jobling, S. 2006, Influence of geotechnical factors on gas flow experienced in a UK longwall coal mine panel. International Journal of Rock Mechanics and Mining Sciences, 43(3), pp.369–387.Wu, J. and Liu, X. 2011, 'Risk assessment of underground coal fire development at regional scale', International Journal of Coal Geology, vol. 86, no. 1, pp. 87–94.

Wu, Z., Jiang, S., He, X., Wang, L. and Lin, B. 2007, Study of 3-D Numerical Simulation for Gas Transfer in the Goaf of the Coal Mining. Journal of China University of Mining and Technology, 17(2), pp.152-157.

Xiang, Z., Si, G., Wang, Y., Belle, B. and Webb, D. 2021, Goaf gas drainage and its impact on coal oxidation behaviour: A conceptual model, International Journal of Coal Geology, 248, p.103878.

Yang, Y., Li, Z., Tang, Y., Liu, Z. and Ji, H. 2014, Fine coal covering for preventing spontaneous combustion of coal pile, Natural Hazards, 74(2), pp.603–622.

Ye, Q., Jia, Z. and Zheng, C. 2017, Study on hydraulic-controlled blasting technology for pressure relief and permeability improvement in a deep hole. Journal of Petroleum Science and Engineering, 159, pp.433-442.

Zhang, C., Tu, S. and Zhao, Y. 2019, Compaction characteristics of the caving zone in a longwall goaf: a review, Environmental Earth Sciences, 78(1).

Zhang, C., Tu, S., Zhang, L., Bai, Q., Yuan, Y. and Wang, F. 2016, A methodology for determining the evolution law of gob permeability and its distributions in longwall coal mines, Journal of Geophysics and Engineering, 13(2), pp.181–193.

Zhao, Y., Yang, T., Zhang, P., Xu, H., Zhou, J. and Yu, Q., 2019. Method for generating a discrete fracture network from microseismic data and its application in analyzing the permeability of rock masses: a case study. Rock Mechanics and Rock Engineering, 52(9), pp.3133-3155.